6-19-2019

Paper-based Point-of-Care Diagnostic Devices for Urinalysis

Fariba Ghaderinezhad
University of Connecticut - Storrs, fariba.ghaderinezhad@uconn.edu

Paper-based Point-of-Care Diagnostic Devices for Urinalysis

Fariba Ghaderinezhad, PhD

University of Connecticut, 2019

Utilizing paper as an easy-to-use and disposable platform for micro analytical devices has garnered considerable attention for point-of-care applications in clinical diagnostics. Moreover, multiplexing these devices enables simultaneous execution of multiple assays on a single device without cross-contamination.

Urine analysis has been used for various diagnostics, including, but not limited to, urinary tract infection (UTI), kidney function, diabetes, pregnancy, and hydration testing. A normal sample of urine consists of several elements: urea, chloride, sodium, amino acids, sulphate, phosphate, potassium, and other trace chemicals, as well as various biomolecules. Abnormal levels of these substances, atypical urine chemical properties, or the presence of certain other chemicals or molecules can be used to diagnose certain health conditions.

According to the World Health Organization (WHO), the most effective way to increase access to medical diagnostics in developing countries is to provide these communities with tools for accessible and affordable local production. In response to this need, in my PhD research, I focused on design and high-throughput fabrication of paper-based microanalytical devices with fast, simple, and cost-effective methods for urinalysis.

For patterning the hydrophobic barriers and high-throughput fabrication of paper-based microfluidics, novel fabrication methods were proposed along with compatible detection methods including colorimetric, electrochemical and fluorescent. First, a pen-plotter-based approach was developed integrated with a custom-made, low-cost paper feeder.

Fariba Ghaderinezhad

University of Connecticut, 2019

Next, the desktop pen plotter was integrated with a 3D-printed custom-designed multi-pen holder for low-cost and multiplexed prototyping of paper-based microfluidics. To continuously supply hydrophobic ink for patterning, a continuous-ink system was implemented and thereby further improve the cost-effectiveness and throughput of fabrication compared to relying on fixed-volume permanent markers. Moreover, to show that this fabrication method is compatible with electrochemical detection methods, a low-cost, high-throughput, single-step fabrication method based on a desktop pen plotter was developed integrated with a liquid dispenser to plot the hydrophobic barriers and the electrodes using carbon paste. Finally, a smartphone-enabled miniaturized paper-based device was designed and fabricated to quantify the concentration of sodium, potassium, calcium, chloride and nitrite ions in urine. Various biochemical assays were conducted using the fabricated devices to validate their application as diagnostic devices.

Paper-based Point-of-Care Diagnostic Devices for Urinalysis

Fariba Ghaderinezhad

B.Sc. Chemical Engineering, Sharif University of Technology, 2009

M.Sc. Chemical Engineering- Biotechnology, Sharif University of Technology, 2011

A Dissertation

Submitted in Partial Fulfillment of the

Requirements for the Degree of

Doctor of Philosophy

at the

University of Connecticut

2019

APPROVAL PAGE

Doctor of Philosophy Dissertation

Paper-based Point-of-Care Diagnostic Devices for Urinalysis

Presented by

Fariba Ghaderinezhad, B.Sc., M.Sc.

Major Advisor_____

Dr. Savas Tasoglu

Associate Advisor_____

Dr. Sharareh Emadi

Associate Advisor_____

Dr. Xinyu Zhao

Associate Advisor_____

Dr. Insoo Kim

Associate Advisor_____

Dr. Anna Tarakanova

University of Connecticut

2019

ACKNOWLEDGEMENTS

I would like to express my appreciation and thanks to my Advisor, Dr. Savas Tasoglu for his support

I also thank Sarah Butters, the best landlord ever because of her endless kindness, great cares, generosity and her gentle soul.

I thank my friends for all their support, their kindness and the fun time that I had with them: Atefeh, Behzad, Ehsan, Farshad, Leyla, Marzieh, Mehdi, Mohammad, Nasrin, Nima, Sara, Shahed, Vida, Abed, Amir, Armin, Ashkan, Bahareh, Farnoosh, Hakimeh, Leila, Mahdi, Nasim, Neda, Reza, and Saman.

I especially thank my parents, Zahra and Iraj, my beloved sister, Fatemeh, and my brothers, Mohammad Hasan and Hamed. Thank you all for being always with me, for supporting me spiritually, for your prays and endless kindness, and for your continuous encouragement throughout my years of study. This accomplishment would not have been possible without you.

TABLE OF CONTENTS

LIST OF FIGURES

LIST OF TABLES

INTRODUCTION

There is an unmet need for a transformation in the healthcare system from reactive and hospital-centered care to a more proactive approach, encompassing preventive, evidence-based, and patient-centered care[1]. To support this much-needed transformation, there is an imminent demand for low-cost, compact, and transformative technologies to perform hourly, daily, or continuous health measurements across the population. Only rigorous scientific innovation can realize such next-generation technologies, which promises to improve patients' well-being, reduction the cost of care, and take on ever present medical challenges.

In the United States alone, healthcare costs are astronomically high and continue to increase every year, exceeding $9,400 per capita in 2014[2]. In 2014, the healthcare expenditure in the United States represented 17.1% of its gross domestic product—the highest healthcare expenditure among all countries in the world. This trend is expected to continue in the coming years. In a study reported by Health Affairs, it was shown that a 90% increase in specific preventative screenings back in 2006 would have saved more than 2 million lives without a significant increase in healthcare costs (in fact, a 0.2% decrease in costs was estimated)[3]. In addition to the improvement in public health, healthcare cost savings could be drastically improved by further research focused on the development and implementation of low-cost preventative care methods and tools. Thus, by enabling and promoting efficient, effective, and affordable preventative medicine, next-generation technologies may prove to be the solution to the ballooning costs of healthcare.

In order to address this need, paper-based devices as diagnostic devices can work well. One of the body fluids which can be used along with these paper-based devices

is urine. Urine analysis has great potential in this respect, considering both its biological richness and its capacity to be a convenient and cost-effective medium for health testing. A large volume of urine is produced daily by the average person: 6–7 urinations totaling 400 to 2000 mL; thus, there is an abundance of samples for collection and analysis[4]. Urine analysis has been used for various diagnostics, including, but not limited to, urinary tract infection (UTI), kidney function, diabetes, pregnancy, and hydration testing[5]. A normal sample of urine consists of several elements: urea, chloride, sodium, amino acids, sulphate, phosphate, potassium, and other trace chemicals, as well as various biomolecules. Abnormal levels of these substances, atypical urine chemical properties, or the presence of certain other chemicals or molecules can be used to diagnose certain health conditions[6].

Utilizing paper as an easy-to-use and disposable platform for micro analytical devices has garnered considerable attention for point-of-care applications in clinical diagnostics, environmental protection and monitoring, food safety testing, chemical education, and forensic analysis. Some particularly attractive advantages of paper-based micro analytical devices are affordability, facile disposability, portability, and simple fabrication which facilitate mass-production[7]. Moreover, multiplexing these devices enables simultaneous execution of multiple assays on a single device without cross-contamination [8]. Sample transportation in paper-based microfluidics is controlled via patterned hydrophobic barriers and propagated by means of the strong capillary action of paper, obviating the need for pumps. Several approaches including photolithography, laser etching, and plasma treatment have been extensively presented with well-characterized materials such as glass, silicon, and polymers for

the fabrication of micro analytical devices. The limitations of these fabrication methods, including lengthiness and the need for expensive instruments and trained personnel, pose challenges regarding ease of mass fabrication and cost-effectiveness in both resource-limited regions and developed countries[9].

Martinez et al. introduced the idea of using paper as a substrate with patterned hydrophobic barriers using a UV-polymerized photoresist[10]. Abe et al. developed a fabrication method based on inkjet printing for creating hydrophilic channels on hydrophobic paper[11]. Over the years, researchers have employed different hydrophobic agents including wax[12,13], permanent marker ink[14], polydimethylsiloxane (PDMS)[15], and alkylketene dimer (AKD)[16,17] for delimiting the barriers.

According to the World Health Organization (WHO), the most effective way to increase access to medical diagnostics in developing countries is to provide these communities with tools for accessible and affordable local production[18]. In response to this need, in my PhD research, I focused on design and high-throughput fabrication of micro paper-based analytical devices (µPADs) with fast, simple, and cost-effective methods for urinalysis.

In this regard, for patterning the hydrophobic barriers and high-throughput fabrication of paper-based microfluidics, a pen-plotter-based approach was developed integrated with a custom-made, low-cost paper feeder (Chapter 1). The capacity of several commercial permanent markers was investigated to produce hydrophobic barriers on delicate task wipers and chromatography papers. To show the effectiveness of this fabrication method, a glucose assay was conducted and colorimetric analysis was used to present the results. Despite the limitations of the colorimetric method, such as inhomogeneity of color distribution and background noise, this quantification method

was employed owing to its easy operation, straightforward signal readout, and the quantifiable results. Since the intensity of the color in detection zones is a function of analyte concentration, quantification of results can easily be performed with a digital camera [7,8]. Therefore, digital image processing was used to locate the detection zones and analyze the color intensities by using a MATLAB image processing scrip. At the next step, the desktop pen plotter was integrated with a custom-designed multi-pen holder for low-cost and multiplex prototyping of paper-based microfluidics (Chapter 2). Permanent markers were used to form a hydrophobic barrier delineating the hydrophilic zones through which the liquid sample travels due to capillary action. The markers were chosen as the patterning agent due to their hydrophobicity and the use of a colorant for visualization of the printed pattern. A custom-designed multi-pen holder was 3D-printed and enabled multiplex plotting. Moreover, a continuous ink system was implemented to continuously supply ink to the technical pens and thereby further improve the cost-effectiveness and throughput of fabrication compared to relying on fixed-volume permanent markers. A laminating layer was incorporated to the fabricated paper-based microfluidic devices to (i) improve their durability, stability, and mechanical strength; (ii) ensure the stability of the hydrophobic barriers and biochemical reagents during storage[19]. To demonstrate the diagnostic applications of resulting paper-based assays, colorimetric tests were conducted for five analytes found in urine: nitrite, urobilinogen, protein, blood and pH.

To overcome the limitation of colorimetric method, and use a detection method with higher sensitivity which is not effected by ambient signals, and to show that this fabrication method is compatible with different detection methods such as electrochemical method,

a low-cost, high-throughput, single-step fabrication method based on a desktop pen plotter integrated with a liquid dispenser was proposed (Chapter 3). Permanent markers and carbon paste were used to plot the hydrophobic barriers and the electrodes, respectively. A syringe was filled with carbon paste and was connected to a liquid dispenser and the paste flow was driven by the application of a fixed air pressure. Also, the paper was hot-laminated on one side to improve its durability, stability, and mechanical strength[20]. The electrochemical operation of the fabricated paper-based assays was validated by chronoamperometry (CA) with potassium ferricyanide. Additionally, CA analysis of glucose was conducted to demonstrate a possible diagnostic application of the fabricated paper-based devices for electrochemical assays.

As the final application, regarding to the importance of measuring the electrolytes including Na^+, K^+, Ca^{2+}, and Cl^- as well as NO_2^- in urine, a smartphone-enabled miniaturized paper-based device was designed and fabricated to quantify the concentration of sodium, potassium, calcium, chloride and nitrite ions in urine (Chapter 4). Deviation of concentration of inorganic ions such as sodium (Na^+), potassium (K^+), calcium (Ca^{2+}), and chloride (Cl^-) from their physiologically accepted healthy ranges, and presence of nitrite (NO_2^-) in human body fluid can be a symptom of a disorder or a dysfunction of an organ. If this is not diagnosed and left untreated, it can lead to serious health issues. Regularly monitoring sodium, potassium and calcium urinary excretion can help to diagnose disorders such as hypertension and cardiovascular diseases, hyperkalemia or hypokalemia (disorders which can be caused by changes in potassium intake), kidney disease or injury, adrenal gland problems, rickets, hypothyroidism, steatorrhea, vitamin D overdose, and renal tubular acidosis. To the best of our knowledge,

for the first time in this field, we used a cost- and time-effective paper-based method for measuring the concentration of Na^+, K^+, Ca^{2+}, and Cl^- ions in urine. For this purpose, fluorescent detection method was chosen for detecting Na^+, K^+, and Ca^{2+} ions and colorimetric method for detecting Cl^- and NO_2^- ions. The reagents on paper matrix was immobilized and after adding the sample, read the fluorescent intensity/ color intensity and quantified the concentration of ions using a plate reader. The fabricated cost-effective mobile fluorescence microscope consists of a 3D-printed housing that aligns with the existing camera module of the smartphone, an external lens, an excitation filter, an emission filter, light emitting- diode (LED), a sample tray, and three batteries. After capturing, the fluorescence image is wirelessly transmitted using a custom-designed smart application to servers for rapid and automated determining the ion concentrations. The digital analysis of the mobile-phone image is based on a machine learning algorithm. The result of this machine-learning-based analysis of each fluorescence image is returned back to the same mobile-phone within ~90 s, and is displayed to the user through the same smart application. This field-portable fluorescent microscopy platform that is integrated on a mobile-phone, together with its machine learning based digital image processing framework, can provide a valuable solution for automated and rapid determining of concentration of ions even in remote and resource limited settings.

1. CHAPTER 1: High-throughput Rapid-prototyping of Low-cost Paper-based Microfluidics

Introduction

Utilizing paper as an easy-to-use and disposable platform for micro analytical devices has garnered considerable attention for point-of-care applications in clinical diagnostics[21,22], environmental protection and monitoring[23,24], food safety testing[25,26,27], chemical education[28], and forensic analysis. Some particularly attractive advantages of paper-based micro analytical devices are affordability, facile disposability, portability, and simple fabrication which facilitate mass-production[7,14,29,30]. Moreover, multiplexing these devices enables simultaneous execution of multiple assays on a single device without cross-contamination[8]. Sample transportation in paper-based microfluidics is controlled via patterned hydrophobic barriers and propagated by means of the strong capillary action of paper, obviating the need for pumps[8,29,31]. Several approaches including photolithography[10,26], laser etching[32,33], and plasma treatment[17] have been extensively presented with well-characterized materials such as glass, silicon, and polymers for the fabrication of micro analytical devices. The limitations of these fabrication methods, including lengthiness and the need for expensive instruments and trained personnel, pose challenges regarding ease of mass fabrication and cost-effectiveness in both resource-limited regions and developed countries[8,14].

Martinez et al. introduced the idea of using paper as a substrate with patterned hydrophobic barriers using a UV-polymerized photoresist[10]. Abe et al. developed a fabrication method based on inkjet printing for creating hydrophilic channels on hydrophobic paper[11]. Over the years, researchers have employed different hydrophobic agents including wax[12,13], permanent marker ink[14], polydimethylsiloxane (PDMS)[15], and alkylketene dimer (AKD)[17,16] for delimiting the barriers. Among these approaches, flexographic[31], and inkjet printing[11,34] are promising for high-throughput and mass

fabrication of paper-based microfluidics[35], due to their advantages of affordability and simple single-step nature[7,14].

In this work, a desktop pen plotter, integrated with a custom-made, low-cost paper feeder (Figure 1-1) was used for single-step patterning of hydrophobic barriers and high-throughput fabrication of paper-based microfluidics. The ability of different brands of commercial permanent markers was investigated to produce hydrophobic barriers on delicate task wipers and chromatography papers. To show the effectiveness of this fabrication method, a glucose assay was conducted and used colorimetric analysis to present the results. Despite the limitations of the colorimetric method, such as inhomogeneity of color distribution and background noise, this method was chosen because of its easy operation, straightforward signal readout, and the quantifiable results[7,34]. Since the intensity of the color in detection zones is a function of analyte concentration, quantification of results can easily be performed with a digital camera[7,8]. Therefore, digital image processing was used to locate the detection zones and analyze the color intensities by using a MATLAB image processing script.

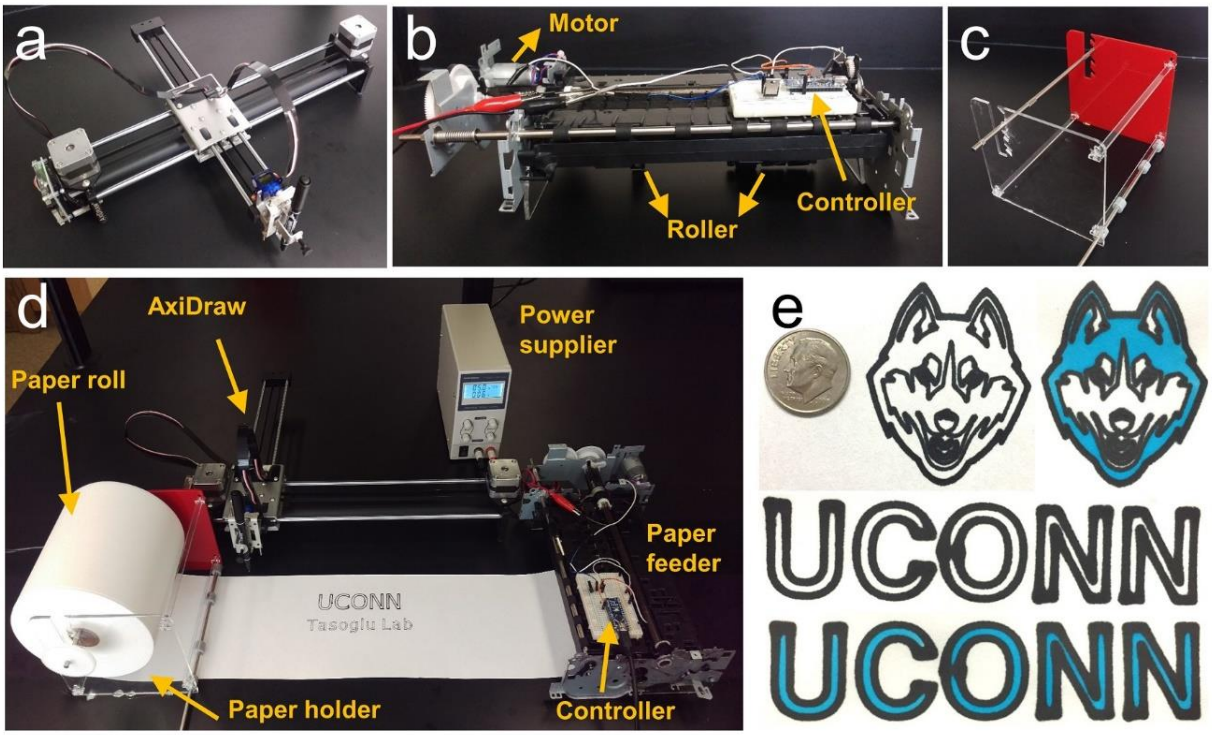

Figure 1-1. High-throughput rapid-prototyping of low-cost paper-based microfluidics. (a) *Desktop pen plotter and* ***(b)*** *a customized paper feeder.* ***(c)*** *Holder of paper roll manufactured with a laser cutter.* ***(d)*** *Plotter integrated with the feeder.* ***(e)*** *Sample patterns plotted by desktop pen plotter and colored by liquid fabric dye.*

Materials and Methods

Materials

A desktop pen plotter, AxiDraw (Evil Mad Scientist Laboratories, CA, USA); Deli markers with different colors (Deli group, Zhejiang, China); Sipa markers with different colors (Sino Path Enterprises Ltd., Guangong, China); Double-ended Comix markers (Comix group Co. Ltd., Shenzhen, China), where the fine-tip and broad-tip markers are 0.5 and 2.0 mm in diameter, respectively; delicate task wipers, KIMTECH (Kimberly-Clark Worldwide, Inc. GA, US); chromatography paper, Whatman No. 1 (GE healthcare life sciences, IL, US); glucose oxidase/peroxidase reagent (G 3660), potassium iodide (793582), trehalose

(PHR1344) all from Sigma- Aldrich, MO, US; pure glucose (Modernist Pantry LLC., NH, US); a microcontroller, Arduino nano (Arduino LLC, US).

Methods

The effects of marker and paper

To investigate the capability of the markers to create hydrophobic barriers resisting aqueous solution, various commercial brands of markers were tested including Sipa (oil-based marker), Deli and Comix (permanent markers). The patterns, circles with a diameter of 4 mm, were prepared with SolidWorks and plotted by AxiDraw pen plotter on two different types of paper (chromatography paper and delicate task wipers). The water-resistant performance of the patterns plotted by six different colors of Sipa markers, two different colors of Deli markers, and one color of double-ended Comix markers (both fine- and broad-tips) were investigated by spotting aqueous solution of yellow food dye in the center of the patterns. To increase the amount of ink diffusing through the paper, multiple passes of plotting were performed.

The effect of plotting speed and pattern dimensions

AxiDraw is a desktop pen plotter with XY resolution of 80 steps per mm, with ±0.1 mm reproducibility, and a maximum plotting speed of 28 cm/s. The speed is adjustable and directly affects the amount of ink diffused through the paper and the feature size of the plotted patterns. A range of speeds from minimum (1%) to maximum (100%) was tested for plotting circles with diameters from 1.6 to 4 mm. Comix (both fine- and broad-tip) and

black Deli markers were tested for this set of experiments as they successfully created hydrophobic barriers.

Paper feeder

To achieve a high-throughput method for fabrication of paper-based microfluidics, a paper feeding mechanism were developed and synchronized with AxiDraw desktop pen plotter. The custom paper feeder was created using a feeder and its motor from an inkjet printer (HP OfficeJet 6500A). The feeder consists of two rollers (1.6 cm in diameter) with a rubber coating to grip the paper. The rollers push the paper down onto the base to keep it inline and level during patterning. An electrical circuit consisting of an external DC power supply, a Mosfet, and a microcontroller is used to control the entire system through a PC. Using an open-loop controlling algorithm, the microcontroller controls the rotation of the motor in accordance with the pattern size and drawing speed. To activate the roller, the electrical circuit is powered by 5 volts and 0.5 amperes, provided by the external DC power supply. The roll of paper is held using a bracket (Figure 1-1c) designed with SolidWorks 2014 (Dassault Systèmes SolidWorks Corp., France) and cut from a 3mm-thick acrylic plate with a CO_2 Laser Cutter (Universal Laser Systems, Inc., AZ, US). The holder and feeder are placed before and after the pen plotter, respectively (Figure 1-1d). The accuracy of the paper feeder was tested to assess its performance. The microcontroller was programmed to run the motor for 1 sec to unravel 10 mm of the paper roll, then stop for 10 sec to allow Axidraw to plot a 5 by 5 mm square. All squares were plotted at the same XY position by sending the plot command via the PC. A Carson eFlex digital camera (Carson Optical, Inc., NY, US) was used to capture images at a fixed

position, focused on the center of the square, for analyzing the position of patterns. 120 repetitions were performed, and the images were analyzed using a MATLAB script (MathWorks, MA, US) to measure the repeatability and accuracy of the feeder.

Glucose assay

To demonstrate the applicability of the proposed fabrication method for paper-based microfluidics in bioassays and verify their effectiveness, a glucose assay was conducted with different concentrations and volumes of glucose solutions (1-50 mM and 1-15 µl). This method relies on the color shift from clear to brown due to the enzymatic oxidation of iodide (I^-) to iodine (I_2). First, glucose is oxidized to produce hydrogen peroxidase (Equation (1)), which can enzymatically oxidize iodide (due to the presence of KI in reagent) to iodine in the presence of horse radish peroxidase (HRP) and produce water as a byproduct (Equation (2))[7,10,36-38].

$$Glucose + H_2O + O_2 \xrightarrow{GO_x} Gluconic\ Acid + H_2O_2 \quad (1)$$

$$Chromogen + H_2O_2 \xrightarrow{peroxidase} Dye + H_2O \quad (2)$$

Using the fine-tip Comix marker, circular patterns with a diameter of 4 mm and plus-shaped patterns with 4 detection zones and 4 channels were plotted on both delicate task wipers and chromatography paper with speeds of 80% and 4%, respectively (Figure 1-4a, d). To show the effect of glucose concentration and solution volume on the resulting color, a range of concentrations (1-50 mM) and volumes (1-15 µl) was tested on circular patterns. Additionally, 7 µl and 35 µl of glucose solution were spotted with different

concentrations onto the center of the plus-shaped patterns plotted on wiper and chromatography paper, respectively. To activate the detection zones, 0.5 µl and 1 µl of the reagent solution (for wipers and chromatography paper, respectively) were spotted in each detection zone and left to dry at room temperature for 10 minutes. The reagent solution includes glucose oxidase/peroxidase reagent (125 units of glucose oxidase enzyme activity and 25 units of peroxidase enzyme activity per ml of solution), 0.3 M trehalose and 0.6 M potassium iodide[10]. Trehalose was added to the reagent mixture as a stabilizer for the proteins in their active form. It has been shown that an absence trehalose yields a loss of enzymatic activity[38].

Results

Water-resistant capability of the markers

Patterns were plotted on both delicate task wipers and chromatography paper with all types of markers used in this study (Figure 1-2a, b). Almost, all the patterns plotted on the front of the chromatography paper are not clearly visible from the back even after three passes (Figure 1-2a, b), showing that the amount of ink was not adequate to diffuse through the paper. However, the patterns on both the front and back sides of the delicate task wiper are almost identical since the wipers have less thickness and less-dense mesh density and ink can diffuse easer. This also explains why most of the circular patterns plotted on the wipers are filled with ink (Figure 1-2a, b). The mesh density of both chromatography paper and wipers has been investigated using SEM imaging (Figure 1-3a). The larger pore size and smaller thickness of wipers explain why inks penetrate better through delicate task wiper than chromatography paper.

The results of testing water-resistant capability of markers demonstrate that, only the patterns plotted with Comix broad-tip markers and 3 passes of Deli black markers are able to resist the aqueous solution on the chromatography paper (Figure 1-2a, b). However, on the delicate task wiper, a single pass of Comix fine-tip or Deli black markers are able to contain aqueous solution of dye within the pattern. Figure 1-2c provides a summary of the performance of all markers used for plotting on two types of paper.

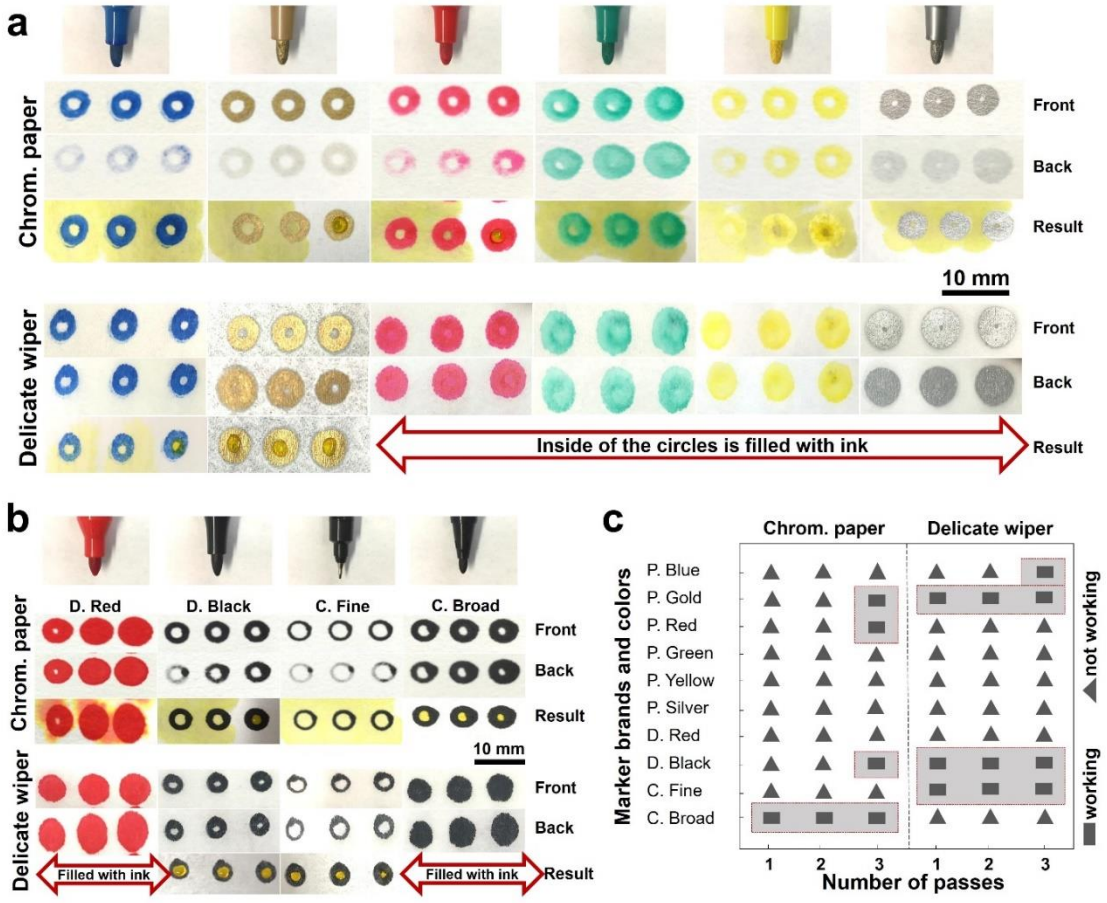

Figure 1-2. The water-resistant capability of markers. (a) *Images of plotted patterns with Sipa markers with different colors on chromatography papers and delicate task wipers. From top to bottom, images were arranged to show the front and the back of the papers (with only inks), and results by spotting aqueous food dye.* ***(b)*** *Images of plotted patterns with Deli and Comix markers on chromatography papers and delicate task wipers.* ***(c)*** *Performance chart for different markers and papers for single and multiple passes. Diameter of the circles is 4 mm.*

The effect of the plotting speed and pattern dimensions

Plotting speed is directly related to the amount of ink that diffuses through the paper. Therefore, the amount of diffused ink can be increase and thereby increase the likelihood of achieving water-resistant patterns by decreasing printing speed. To show the penetration of the ink through the paper, lines on chromatography paper were first plotted with different plotting speed and number of passes, and then the cross-sections were demonstrated using optical microscope (Figure 1-3b). Figure 1-4a shows that plotting on chromatography paper using Comix fine-tip markers at speeds less than 5% yield water-resistant patterns, and if the number of passes were increased to 3, water-resistant patterns can be achieved at a speed as high as 30%, which is similar to the results for Deli black markers. However, using Comix broad-tip markers for plotting can produce water-resistant patterns at all speeds. Figure 1-4b summarizes the performance of Deli black and both fine- and broad-tip Comix markers for creating hydrophobic barriers on chromatography paper. The same experiments were performed with Comix fine-tip and Deli black markers on delicate task wipers, which resulted in water-resistant patterns for all tested speeds. These two markers were chosen for testing on delicate task wipers because all other marker types yielded ink-filled patterns. The results of this experiment are presented in Figure 1-4c. Moreover, the viscosity and contact angle of the Comix and Deli black inks were measured. The results are presented in Table 1-1 and Figure 1-3c,d,e. Contact angle of the surface covered with Deli ink is less than that of covered by Comix which confirms that Comix ink is more hydrophobic and acts as a better hydrophobic barrier in spite of its less viscosity.

Table 1-1: Viscosity and contact angle of Comix and Deli ink

	Comix	Deli
Viscosity (cp) at 23 °C	4.43 ± 0.04	5.94 ± 0.07
Contact angle on chromatography paper	127.6 ± 5.3	9.1 ± 2.6
Contact angle on wiper	119.6 ± 8.8	86.2 ± 5.3

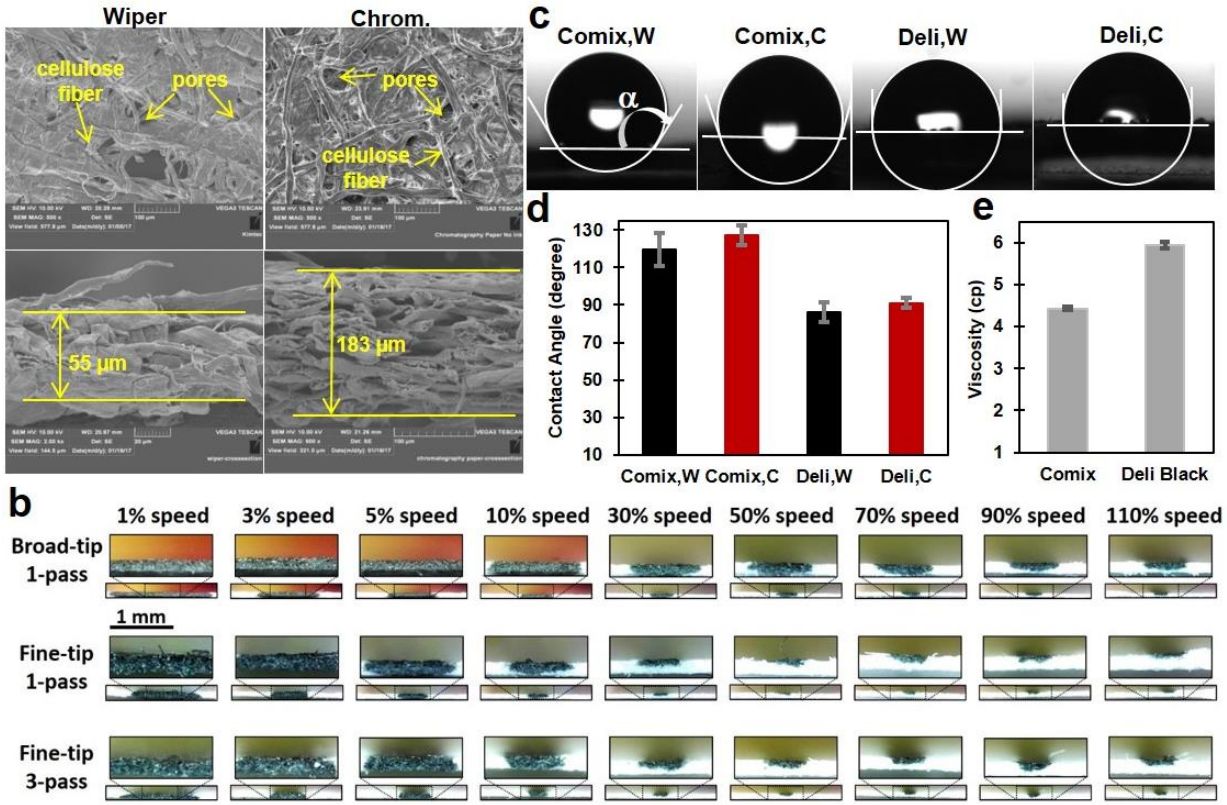

Figure 1-3. Characterization of paper substrates and inks. (a) *SEM images of the surface and cross-section of delicate task wipers and chromatography paper.* ***(b)*** *Diffusing ink through chromatography paper at different plotting speeds from 1% (smallest speed) to 110% (largest speed), and number of passes using fine and broad-tip of Comix marker.* ***(c)*** *Images of a 2-µl-droplet on different substrates covered with the inks. C and W stands for chromatography paper and Wipers, respectively.* ***(d)*** *Contact angle of a 2-µl-droplet on substrates covered with Comix and Deli ink (data are average of left and right contact angles).* ***(e)*** *Viscosity of Comix and Deli inks at 23 °C. Measurements are average of six repeats for both contact angle and viscosity.*

In addition to investigating the effect of plotting speeds, circles with different diameters (from 1.6 mm to 4 mm) were plotted to determine the resolution achievable with AxiDraw while still producing water-resistant patterns. Figure 1-4d shows the patterns at different

sizes and speeds on delicate task wipers plotted with a Comix fine-tip marker. Results showed that the smallest feature which can be plotted without being filled with ink is a circle with a diameter of 2 mm.

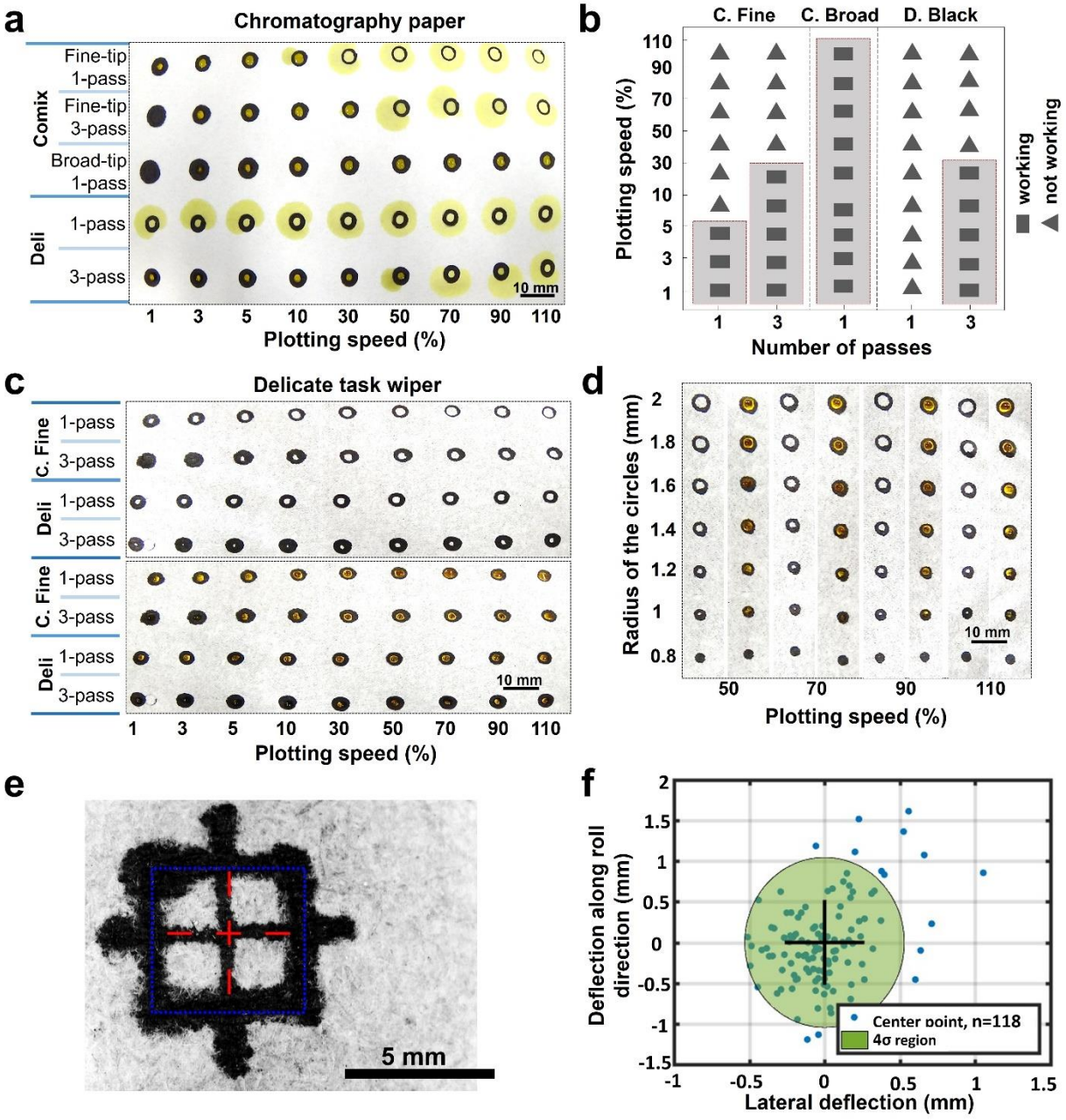

Figure 1-4. Investigating the effect of plotting speed and pattern dimensions. *Comparing different plotting speeds, markers, and number of passes on* ***(a)*** *Chromatography paper and* ***(b)*** *its summarized results as a performance chart.* ***(c)*** *Comparing different plotting speeds, markers, and number of passes on delicate task wiper.* ***(d)*** *Testing different plotting speeds and pattern dimensions with Comix fine-tip marker on delicate task wipers with a single pass.* ***(e)*** *A sample of an image processed pattern used for repeatability assessment.* ***(f)*** *Deviation of the plotted pattern from the center of the plotter origin.*

Paper feeder

The result of the paper feeder accuracy test is obtained by plotting the pattern shown in Figure 1-4e, and using image analysis to detect the location of the pattern. The results of this experiment are shown as a scatterplot in Figure 1-4f. Each data point in this graph shows the deviation of the center of a pattern relative to the average center position for all patterns. The shaded region indicates the data-points with less than 4σ deviation deflection. Data points falling outside of the green circle in this scatterplot indicate misalignment of the paper being fed due to interference from the markers. Specifically, the paper was not adequately clamped to the base; this allowed the friction produced between the paper and the moving marker tips, which are soft felt, to drag the paper, causing shaking and misalignment. Misalignments can be explained by a number of other factors as well, including the surface roughness of paper and the coefficient of friction between the base and paper. The base has a very smooth surface and low coefficient of friction, allowing the paper to be more easily dragged by the marker tip, which has a higher coefficient of friction. It is important to consider the effect that the surface of the base has on the paper.

Glucose assay

To verify the effectiveness of the presented method for fabrication of paper-based microfluidics, a glucose assay was conducted on two different types of paper using colorimetric analysis. Glucose solutions with different concentrations (1, 2.5, 5, 10, 20 and 50 mM) and volumes (1, 2, 3, 5, 7, 10 and 15 µl) were used to show the effect of concentration and volume on color intensity. Figure 1-5a clearly shows that increasing

either concentration or volume of the glucose solution increases color intensity. In the next step, the similar experiments were done at different concentrations of glucose but with a constant volume (2 µl and 5 µl for delicate task wipers and chromatography paper, respectively) and also at different volumes of solution with constant glucose concentrations (2.5 mM and 20 mM). The quantified results of these sets of experiments are presented in Figure 1-5b, c, which clearly confirm the direct relationship between color intensity and concentration and volume.

To verify the multiplexing capability of the presented fabrication method in simultaneously running multiple assays on a single device without cross-contamination, the plus-shaped patterns with four detection zones were used. Two of the detection zones were spotted with the glucose reagent and two of them were the designated controls (one with the reagent solution without potassium iodide (KI) and one with no solution). Figure 1-5d shows that color formation is only observed in the detection zones with the glucose reagent; the control zones were not affected. Figure 1-5e, f are the quantified results of Figure 1-5d, in which R1 and R2 are the ratio of the intensity of detection zone 1 and 2 to paper, respectively and R3 is defined as the intensity ratio of detection zone 3 to 4; since the experimental conditions of the zone 3 and 4 were the same, R3 was expected to be around 1.

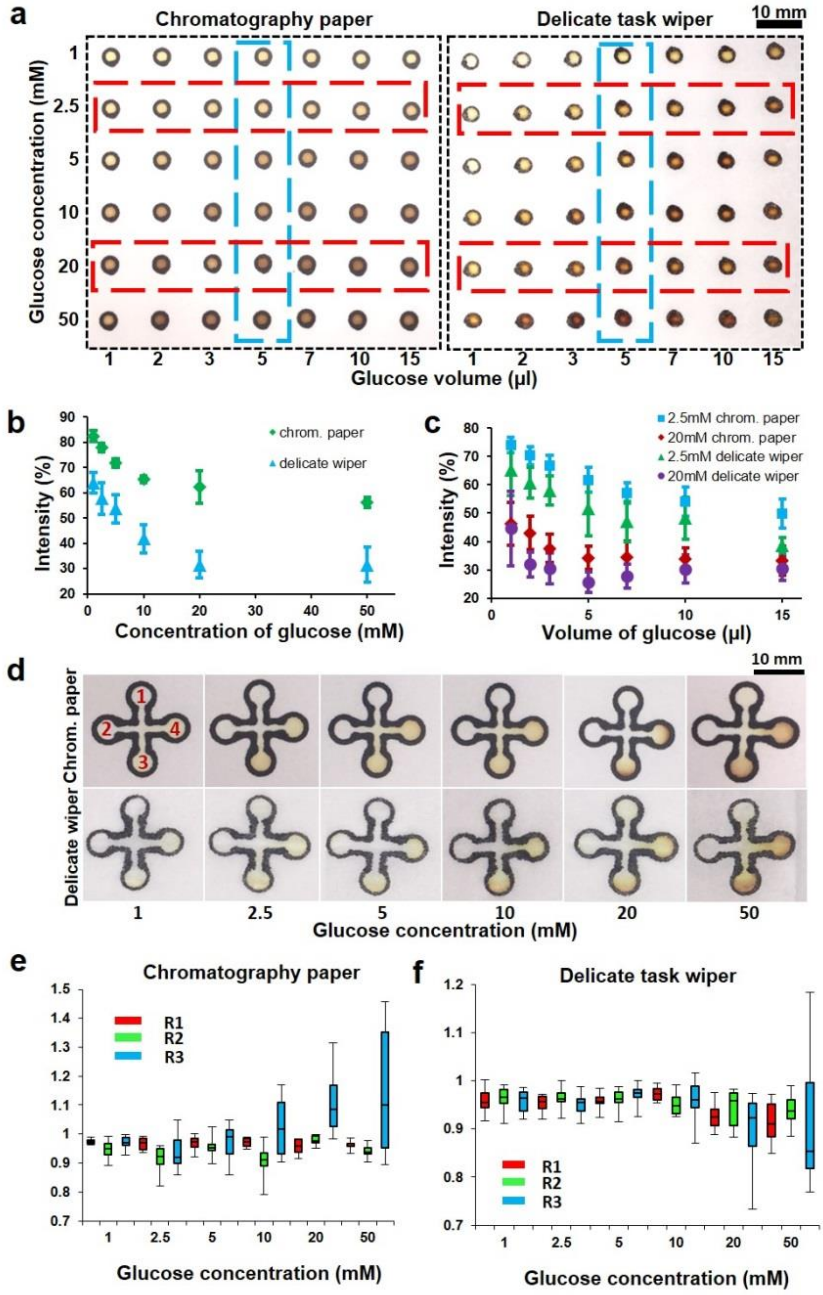

Figure 1-5. Glucose assay via calorimetric method. (a) *Effect of glucose concentration and volume on color intensity.* ***(b)*** *The quantified results of the effect of glucose concentration on color intensities at constant volumes of 5 µl and 2 µl for chromatography paper and delicate task wipers, respectively.* ***(c)*** *The quantified results of the effect of glucose volume on color intensities at concentrations of 2.5 mM and 20 mM on both chromatography paper and delicate task wipers.* ***(d)*** *Glucose assay tested at different concentrations on plus-shaped patterns on both chromatography paper and delicate task wipers and* ***(e,f)*** *their quantified results. Zone 1 is blank, zone 2 has reagent without KI, and zones 3 and 4 has dried reagent. R1 and R2 are the intensity ratios of zone 1 and zone 2 to the paper* (i.e. *blank paper color intensity quantified at the outside of plus-shaped patterns using the same image to cancel out the ambient light effects), respectively and R3 is the intensity ratio of zone 3 to zone 4.*

Discussion

Permanent marker inks are usually water-resistant and contain a hydrophobic resin, a solvent (typically ethanol), and a colorant[39]. Patterns were plotted onto chromatography paper and delicate task wiper using permanent markers, and the ink was allowed to penetrate completely through the paper. Chromatography paper was selected because of its uniform thickness and wicking properties while delicate task wipers have a favorably high wicking speed. Based on the commercial information, the thickness of chromatography paper used here is 180 µm, which is consistent with the presented SEM images (Figure 1-3a). The information of delicate task wipers is not commercially available. The results showed that thickness of wipers is 55 µm. Based on all this information, it can be concluded that the less thickness and larger pore size of the wipers result in better penetration of the ink through the thickness to create barrier.

After evaporation of the solvent, the hydrophobic resin and the colorant remain in the paper and create a hydrophobic barrier throughout the thickness of the paper. Aqueous samples are contained within the hydrophilic zones delimited by the hydrophobic barriers. To assess the water resistance of the permanent markers, aqueous dye was added to circular patterns plotted on both the delicate task wipers and chromatography paper using a desktop pen plotter. As shown in Figure 1-2, Comix broad-tip markers on chromatography paper and Comix fine-tip and Deli black markers on delicate task wipers produced sufficiently hydrophobic barriers capable of containing the aqueous dye. However, Deli red and almost all colors of Sipa markers were unable to either effectively resist the aqueous solution on chromatography paper or create unfilled circles with diameter of 4 mm on the delicate task wipers.

Figure 1-4 shows that Comix broad-tip markers can successfully create hydrophobic patterns at different speeds with a single pass on the chromatography paper, whereas Deli black marker can resist the aqueous sample only at speeds lower than 30% and with 3 passes of printing; this disparity may be due to the difference in hydrophobicity of the marker inks resulting from the variation in composition. The fine-tip of Comix marker produced patterns on the chromatography paper successfully resisted aqueous solution at speeds lower than 5% with a single pass and speeds lower than 30% with 3 passes. The fine-tip Comix marker only works at low speeds because it deposits an insufficient amount of ink that is unable to diffuse entirely through the paper. Moreover, based on the results in Figure 1-4, Comix fine-tip markers can be used to have features as small as 2-mm-diameter circles. By considering the overall performance of the markers, fine- and broad-tip Comix markers were selected to continue the experiments to demonstrate high-throughput microfluidics fabrication with an Axidraw plotter.

To show an application of the presented fabrication method in bio-chemical analysis field, glucose assay was conducted. Results (Figure 1-5) demonstrate that the device is capable of showing a direct relation between the glucose amount (e.g. by changing both concentration and volume) and resulting color intensity. Figure 1-5e, f shows the multiplexing ability of the presented method for running simultaneous assays. However, it should be noted that the volume of the spotted sample plays an important role and it should be optimized depending on the type of the paper for preventing the cross-contamination issue.

Conclusion

Choosing an appropriate patterning method for mass fabrication of paper-based microfluidics requires a trade-off among cost, convenience, and resolution. We have demonstrated an inexpensive, high-throughput, simple, and rapid prototyping method for fabrication of paper-based microfluidics by using a desktop pen plotter, a customized paper feeder, and a permanent marker on delicate task wipers and chromatography paper. With the proposed technique, the fabrication cost of a 10 cm by 100 cm paper microfluidic strips is less than $1 and takes less than 15 min. To demonstrate the potential applications of this fabrication method in biological and chemical analysis, a glucose assay was performed, and the results were quantified. The ink capacity of the commercial permanent marker may be considered as a drawback of this technique regarding mass production, but that could easily be addressed by supplying the marker with a larger ink reservoir. Furthermore, an empty marker could be used for dispensing bioreagents onto the detection zones of paper microfluidics. By considering the cost and resolution offered by this fabrication method as well as ease of fabrication, this approach is a highly-suitable in fabrication of paper-based microfluidics for different applications including point-of-care diagnostics, food safety monitoring, and environmental testing, especially in poor-resource areas.

2. CHAPTER 2: A Continuous-ink, Multiplexed-pen Plotter Approach for Low-cost, High-throughput Fabrication of Paper-based Microfluidics

Introduction

Micro-analytical devices provide point-of-care diagnostics in a multitude of disciplines[40-45], including, but not limited to, the medical field[21,25,46-59], environmental and food safety[23-27], chemical testing[28], and forensic analysis[60]. Microfluidic devices can greatly benefit from low-cost, readily-available materials as well as simple and rapid fabrication processes. Specifically, paper-based microfluidic devices offer a low-cost, high-throughput, and disposable alternative[7,29,30,61] due to their affordability and ease of manufacturing[7]. Several approaches to high-throughput fabrication of paper-based microfluidic devices have been recently presented[16,31,34,35,62].

According to the World Health Organization (WHO), the most effective way to increase access to medical diagnostics in developing countries is to provide these communities with tools for accessible and affordable local production[18]. In response to this need, an approach was developed using a desktop pen plotter integrated with a custom-design multi-pen holder for low-cost and multiplex prototyping of paper-based microfluidics. Permanent markers were used to form the hydrophobic barrier delineating the hydrophilic zones through which the liquid sample travels due to capillary action. The markers were chosen as the patterning agent due to their hydrophobicity and the use of a colorant for visualization of the printed pattern[39]. A custom-designed multi-pen holder was 3D-printed and enabled multiplex plotting (Figure 2-1a,b). Moreover, a continuous ink system was implemented to continuously supply ink to the technical pens and thereby further improve the cost-effectiveness and throughput of fabrication compared to relying on fixed-volume permanent markers (Figure 2-1c,d). A laminating layer was incorporated to the fabricated paper-based microfluidic devices to (i) improve their durability, stability, and mechanical

strength; (ii) ensure the stability of the hydrophobic barriers and bio-chemical reagents during storage[19]. To demonstrate the diagnostic applications of resulting paper-based assays, colorimetric tests were conducted for five analytes found in urine: nitrite, urobilinogen, protein, blood and pH.

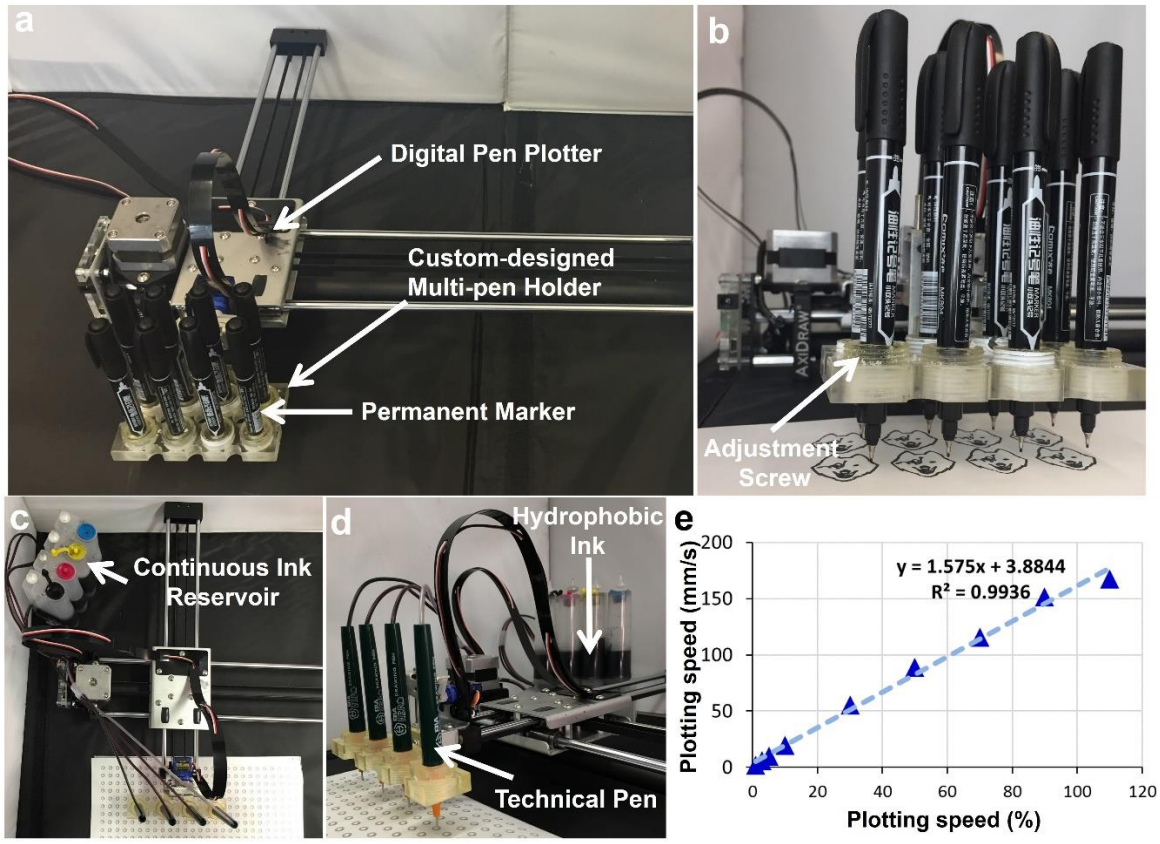

Figure 2-1. A multi-pen plotter for fabricating paper-based microfluidics. (a) *Desktop pen plotter integrated with custom-designed multi-pen holder.* ***(b)*** *Low-cost, 3D-printed multi-pen holder, which was custom-designed to increase the throughput of the setup.* ***(c)*** *Top-view and* ***(d)*** *side-view of the continuous ink system (Ink reservoir) integrated to the pen plotter with multi-pen holder.* ***(e)*** *Plotting speed mm/s vs. percentage; Linear velocity (mm/s) was calculated by measuring the time needed for plotting a 25-cm line with a fine-tip Comix marker.*

Materials and Methods

Materials

Hardware setup: A desktop pen plotter, (AxiDraw) from Evil Mad Scientist Laboratories, CA, US; Double-ended Comix marker from Comix Group Co. Ltd., Shenzhen, China, where the fine and broad tip ends used are 0.5 and 2.0 mm in diameter, respectively; Chromatography paper (Whatman No. 1) from GE healthcare life sciences, IL, US; Objet 30 Prime 3D printer from Stratasys Ltd., MN, US; Ink reservoir (DIY CISS Continuous Ink Supply System) from BCH Technologies, NC, US; Technical drawing pen (1.2 mm) from Shanghai Hero Plotter instrument Co., Shanghai, China; Cold-laminating layer (self-adhesive laminate sheets) from Fellowes, IL, US; Hot-laminating layer (GBC EZUse thermal laminating Pouches) from Swingline, IL, US; Benchtop laminator (GBC Inspire) from Swingline, IL, US; Super hydrophobic solution from NeverWet LLC, PA, US; Aniline dye stain (Oil soluble) from J.E. Moser's, WY, US.

Reagents for biological assays: Sulfanilamide (S9251), N-(1-naphthyl) ethylenediamine dihydrochloride (33461), Citric acid (251275), Sodium nitrite (237213), 4-diethylaminobenzaldehyde (156477), Tetrabromophenol blue (199311), Bovine Serum Albumin (BSA) (A7906), Cumene hydroperoxide (247502), 3,3’,5,5’-tetramethylbenzidine (TMB) (860336), Methyl red sodium salt (114502), Bromothymol blue (114413), Sodium hydroxide (S8045), Hydrochloric acid (258148), Potassium phosphate buffer, pH 6 (01476), Buffer solution pH 9 (456101) all from Sigma- Aldrich, MO, US; Phosphate buffer saline (10010023) from Thermo Fisher Scientific Inc., MA, US; Urobilinogen (sc-296690) from Santa Cruz Biotechnology, TX, US.

Methods

Design and 3D printing of the multi-pen holder

To increase the throughput of patterning for fabrication of paper-based microfluidics, a low-cost multi-pen holder was custom-designed and printed it using a polyjet 3D printer. The 3D-printed multi-pen holder is able to hold 8 pens to plot 8 patterns at the same time. To investigate the accuracy of the Axidraw pen plotter integrated with the multi-pen holder, circles with diameters of 4 mm were plotted by both fine and broad tips of the Comix marker at different plotting speeds. Images of the patterns were captured and analyzed using a MATLAB script (MathWorks, MA, US) to measure the deflection of each pen as well as the deflection of the whole plotting system at different plotting speeds in both the X- and Y-directions. Moreover, the roundness and uniformity of the plotted circles was investigated by measuring their inner and outer radii. A MATLAB script was used to measure the inner and outer radius of each circle at 8 different points (at angles of 0, 45, 90, 135, 180, 225, 270 and 315 degrees) and the average and standard deviation of the radii for each circle were reported.

Lamination of the paper

The fabricated paper-based microfluidic device is comprised of chromatography paper patterned with hydrophobic resin and backed with a laminating layer to seal the device and improve its mechanical strength. To investigate the effectiveness of the laminating layer to seal the back of the chromatography paper, two different lamination methods have been tested: cold- and hot-lamination. Cold-laminating and hot-laminating layers were aligned on the back of the chromatography paper and laminated with a benchtop

laminator in cold and hot modes, respectively. The performance of the plotted patterns on both hot- and cold-laminated papers was studied in two different cases: plotting patterns before and after the lamination. A matrix of circles with a diameter of 4 mm was prepared with SolidWorks 2014 (Dassault Systèmes SolidWorks Corp., France) and plotted by the AxiDraw pen plotter on both hot- and cold-laminated papers. Different plotting speeds ranging from 1% to 110% were tested with varying repetitions (1, 3, and 5 passes over the same pattern). The water resistance of the patterns on the laminated paper was investigated by spotting a dyed aqueous solution in the center of each circle. Moreover, to investigate the mechanical strength of the laminated papers, tensile tests were performed based on ASTM D638 standard for a type-IV specimen. The hot- and cold-laminated papers were cut and tested by a universal testing machine (eXpert 3910, ADMET, MA, US). Furthermore, to study the mechanical strength of the laminated paper after loading an aqueous sample, a tensile test was performed on patterns that had been loaded with 20 µl of dyed aqueous solution at the center of circle.

Continuous ink supply

To improve the limited ink capacity of the commercial permanent markers, a continuous ink supply system was developed and connected to technical pens. The ink reservoir was connected to the cartridge of a technical pen by tubing. The air release hole of the technical pen was blocked to seal the technical pen reservoir from the atmosphere and thereby generate negative pressure in the technical pen reservoir as the ink is depleted while plotting (Figure 2-4a). This negative pressure in the technical pen chamber causes a flow of ink from the main ink reservoir to the technical pen reservoir. A hydrophobic ink

was prepared by dissolving an oil-soluble dye in super-hydrophobic solution. The components of NeverWet hydrophobic ink are given in the Table 2-1. The performance of the prepared hydrophobic ink in the continuous ink system was then studied by patterning the chromatography paper with different plotting speeds and investigating the water resistance of the resulting patterns.

Table 2-1. The components of the hydrophobic ink

Chemical Name	Weight %
Mineral Spirits	<90.0
Aromatic Petroleum Distillates	<10.0
Naphthalene	<1.0
Aniline Dye Stain	<1.0

Colorimetric biological assays

To demonstrate the applicability of the proposed fabrication method for paper-based microfluidics and to verify their effectiveness, five colorimetric assays[40-42] were conducted: nitrite, urobilinogen, protein, blood, and pH (Table 2-2). 0.5 µl of the reagent solution was spotted in the detection zone and left to dry at room temperature for 10 minutes. Each sensor was then validated by applying 3 µL of an artificial urine sample, (engineered with varying concentrations of each analyte in a physiologically relevant range) and measuring the color the change at each concentration.

Table 2-2. Colorimetric reagents, color change reaction, and physiologically-relevant analyte range

	Nitrite assay[40]
Reagents	50 mM sulfanilamide, 10 mM N-(1-naphthyl) ethylenediamine dihydrochloride, 330 mM citric acid
Reaction	Sulfanilamide + NO_2^- $\xrightarrow{acid}$ Diazonium salt Diazonium salt + N-(1-naphthyl)ethylenediamine → Magenta azo dye
Analyte range	0.078, 0.156, 0.312, 0.625, 1.25, and 2.5 mM
	Urobilinogen assay[42]
Reagents	0.1 M 4-(Dimethylamine)benzaldehyde
Reaction	Urobilinogen + 4-(dimethylamine)benzaldehyde $\xrightarrow{acid}$ Pink azo dye
Analyte range	0.2, 1, 2, 4, 8, and 12 mg/dL
	Blood assay
Reagents	6.6% w/w cumene hydroperoxide, 4.0% w/w 3, 3', 5, 5'-tetramethylbenzidine
Reaction	cumene hydroperoxide + 3,3',5,5'-tetramethylbenzidine $\xrightarrow{hemoglobin}$ 3,3',5,5'-tetramethylbenzidine diimine (blue)
Analyte range	2.5, 5, 10, 25, 50, 80, 100, 200 red blood cells/µL
	Protein assay[41]
Reagents	3.3 mM tetrabromophenol blue, 250 mM citric acid
Reaction	Based on the protein error of indicators, where protein alters the color of acid-base indicators without changing the pH of the solution by accepting hydrogen ions from the indicator
Analyte range	15, 30, 100, 300, 2000 and 2500 mg/dL bovine serum albumin
	pH assay[42]
Reagents	0.02% methyl red sodium salt 0.25% of bromothymol blue
Reaction	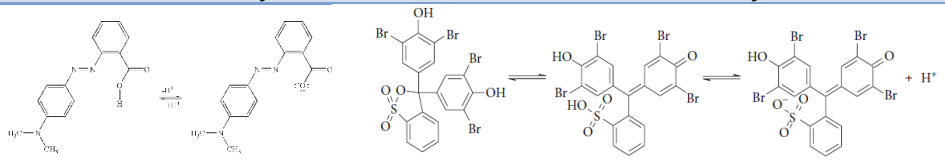 Yellow Red || Yellow Green Blue
Analyte range	pH 5, 6, 7, 8, and 9

Results and Discussion

Design and 3D printing of a multi-pen holder

To increase the throughput of the fabrication, a multi-pen holder was designed to align 8 markers such that they would connect to the plotter and plot a single pattern in parallel (Figure 2-2a). The height of each marker can be separately adjusted precisely using threaded fittings on the pen holder to make the pressure of each pen on the paper consistent and decrease the deflection of the pen against the paper (Figure 2-1b). As the

speed of the plotter can be adjusted based on the percentage of the maximum linear speed, the non-dimensional unit (%) was converted o linear speed (mm/s) (Figure 2-1e); therefore, 30% speed is equivalent to 55.3 mm/s.

To characterize the accuracy of the plotting at 30% plotting speed, a pattern of 12×12 circles was plotted by both the fine- and broad-tip Comix markers (Figure 2-2b). The trueness and the precision of this process were measured. X and Y are defined for each marker as the error in the plotting (i.e. the deviation of the center of the plotted circle from the position defined in the design) in the X- and Y-directions, respectively. $\overline{X}$ and $\overline{Y}$ are the averages of X and Y over the set of eight markers, including twelve trials. Therefore, $\overline{X}$ and $\overline{Y}$ represent the trueness of the plotting approach. These values are 0.40 mm and 0.55 mm for the fine tip, respectively and 0.40 mm and 0.54 mm for the broad tip, respectively.

The precision in the X- and Y-directions can therefore be defined as X-$\overline{X}$ and Y-$\overline{Y}$. The results of twelve circles plotted with eight different markers were plotted and a 95% confidence ellipse was plotted using the 2σ values in the X- and Y- directions (Figure 2-2c, e). The ellipse for the fine tip (0.80 mm by 1.22 mm in the X- and Y-directions, respectively) is larger than that of the broad tip (0.45 mm by 1.11 mm in the X- and Y-directions, respectively), indicating that a greater precision can be attained with the broad tip. The results show that the pens which are farther from the support (Pen 1, 4, 5 and 8) have a larger deflection in both the X- and Y-directions. This may be partially due to the lower stability of the holder in the corners, which allows more deflection when the markers meet the paper.

The deflections of the circles plotted using the fine-tip and broad-tip of the single marker plotting vs. the eight markers plotting have been investigated. The results showed that the accuracy of the single marker drawing is higher than the accuracy of the eight markers drawing. The trueness of the single pen plotting approach is measured to be -0.02 mm and 0.14 mm for the fine tip, and 0.06 mm and -0.43 mm for the broad tip, in X- and Y-direction respectively. The 2σ values (95% confidence ellipse) in the X- and Y- directions have been calculated to be 0.36 mm by 0.28 mm respectively for the fine tip and 0.39 mm by 0.27 mm respectively for the broad tip.

The effects of different plotting speeds on the accuracy were also quantified. Figure 2-2d,f displays the deflection of the patterns plotted at different speeds with both the fine and broad tips. The results show that the deflection for both tips is in the same range; furthermore, the speed has little influence on the deflection which means that the multi-pen holder could work well at different plotting speeds. The plotting speed does not significantly affect the accuracy and precision of the plotting.

The roundness of the plotted circles was also investigated. The inner and outer radii of the circles were measured at 45° intervals using a MATLAB script, as shown in Figure 2-2g. Figure 2-2h,i show the inner and outer radii of the plotted patterns as a function of plotting speed for the fine and broad tips. The standard deviation in the plotted radii is a measure of roundness: the roundness is better when using the fine tip. The roundness decreases significantly at lower plotting speeds and plateaus around 30% plotting speed. The line thickness is also shown as the difference between the inner and outer radii. Further, plotting speed affects the time the marker spends in contact with the paper and, therefore, the amount of ink deposited. As expected, by increasing the plotting speed, the

inner and outer radii of the circles decrease, resulting in a smaller line thickness; the thickness plateaus at speeds more than 30%.

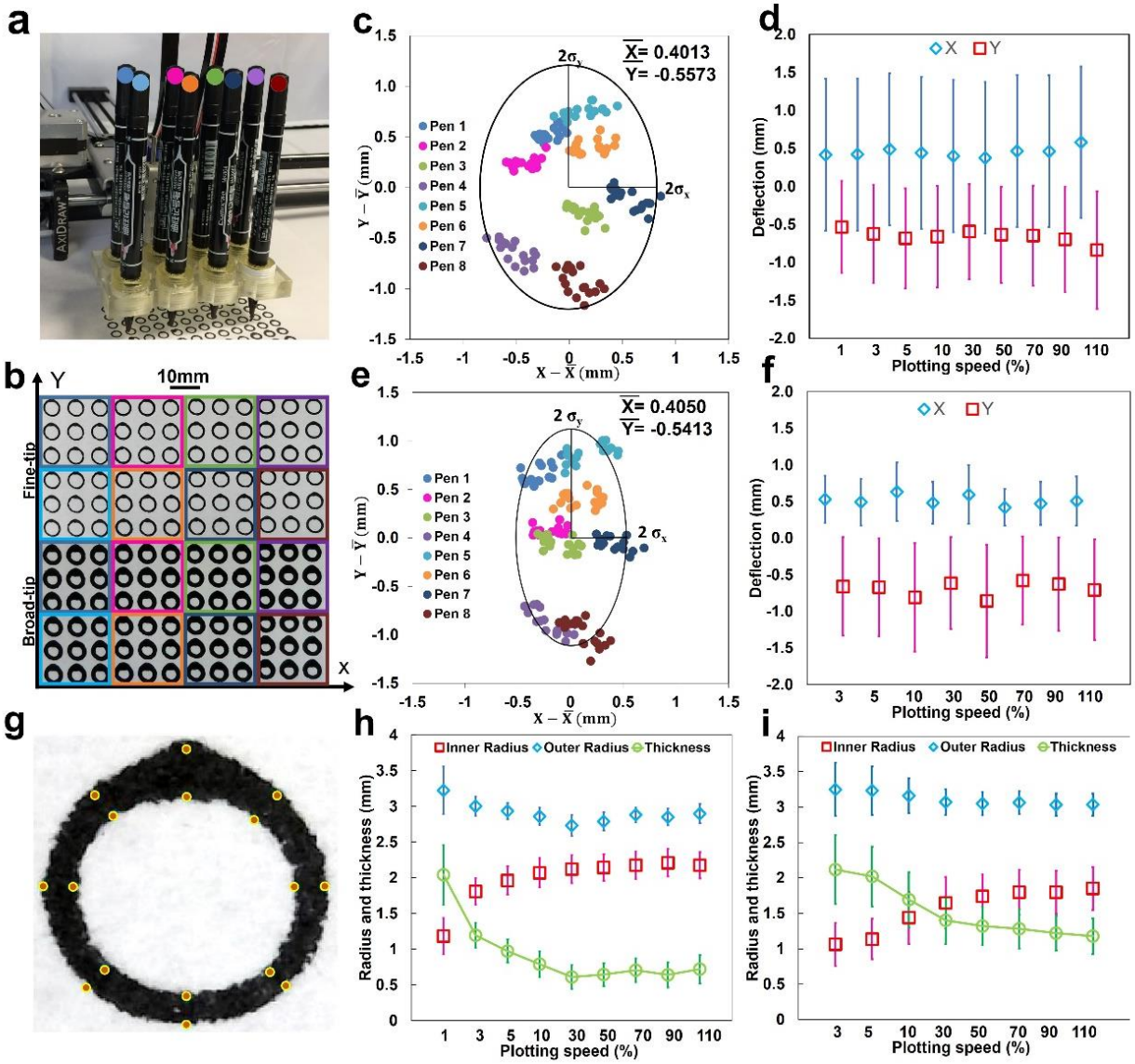

Figure 2-2. Accuracy of plotted patterns using multi-pen holder with eight pens. (a) *Custom-made, 3D printed multi-pen holder integrated with pen plotter.* ***(b)*** *Printed circle pattern with the both fine- and broad-tips of Comix marker using multi-pen holder.* ***(c)*** *Deflection of the plotted patterns with fine-tip of eight Comix marker in both the X-and Y-directions.* ***(d)*** *The mean and standard deviation (STD) of deflection of the plotting system (all eight pens) when plotting with fine-tip at different plotting speeds (n=9).* ***(e)*** *Deflection of the plotted patterns with the broad-tip of eight Comix markers in both the X- and Y-directions.* ***(f)*** *The mean and standard deviation (STD) of deflection of the plotting system (all eight pens) when plotting with broad-tip of marker at different plotting speeds (n=9).* ***(g)*** *Representative method of measuring the inner and outer radius of plotted circles at eight different points (at angle of 0 to 315 with the interval of 45 degree) with MATLAB scripts. The mean and standard deviation of inner and outer radius of the plotted patterns at different plotting speeds with the* ***(h)*** *fine-tip and* ***(i)*** *broad-tip of the Comix marker.* σ_x,

σ_y are the total standard deviation in X- and Y-direction, respectively. $\bar{X}$ and $\bar{Y}$ are the mean deflection in X- and Y-direction, respectively.

Lamination of the paper

While the paper used here is made of cellulose, which loses its mechanical properties upon wetting, a lamination layer was implemented on the back face of the paper (opposite the patterned side) to improve the durability, stability and mechanical strength. Figure 2-3a shows the SEM image of a cross-section of the paper with a hot- and cold-lamination layer. The difference between plotting the patterns were investigated before and after laminating the papers and compared their performance at different plotting speeds using both fine and broad tips. circles with a diameter of 4 mm were plotted and used a dyed aqueous solution to test the water resistance of the patterns. The results are presented in Figure 2-3b and are summarized in Figure 2-3c. The results of the two studied cases (plotting before and after laminating) are very similar, which gives flexibility to the fabrication process (i.e. patterning and lamination may be performed in any order). Moreover, a fatigue test (engineering stress and strain test) was done on the both hot- and cold-laminated papers and compared the results with the plain paper. These experiments were performed under two different conditions: when the laminated papers were wet, and when they were dry. Figure 2-3d shows the stress-strain curve, yield strain and stress, and ultimate strain and stress of these five different samples. The results show that, by laminating the chromatography paper, the yield stress can be improved around 3 times with hot lamination and 1.5 times with cold lamination. This enhancement in strength is more critical after wetting, which simulated an applied sample: the wet chromatography paper could not tolerate the stress, but the laminated papers could bear

larger stress. Wetting the laminated papers reduced their yield stress by 25%-35%, but this strength is still greater than that in the non-laminated wet paper.

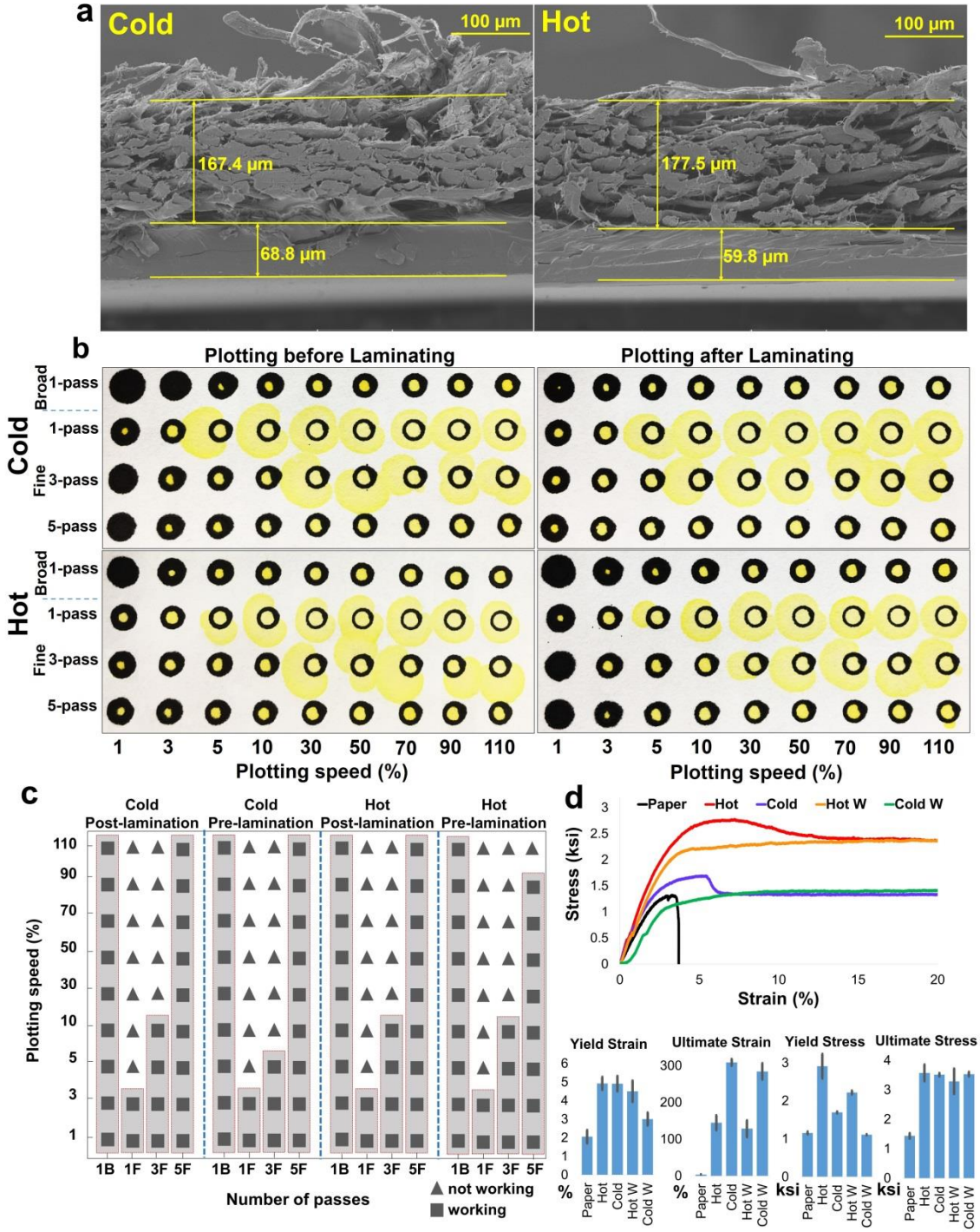

Figure 2-3. The characteristics of the laminating layer and its effect on the performance of the fabricated device. (a) *SEM image of the cross section of hot- and cold-laminated papers* ***(b)*** *Effect of different plotting speeds and number of passes on water resistance of patterns before*

and after laminating the paper. ***(c)*** *The summarized results as a performance chart.* ***(d)*** *Stress-Strain test of laminated papers.*

Continuous ink supply

A continuous ink supply system (Figure 2-1c,d) was developed to improve the cost-effectiveness and throughput of the fabrication. For this purpose, a commercially-available hydrophobic solution has been dyed and used as the plotting agent. The ink was fed continuously into the technical pens (Figure 2-4a), which were contained in a multi-pen holder (Figure 2-4b). The setup was used to plot patterns in both the non-continuous (using the internal cartridge of the technical pen) and continuous flow systems at different speeds. The water resistance of the prepared ink was investigated to confirm that the patterned hydrophobic barriers can effectively contain an aqueous sample in the hydrophilic testing region. The results in Figure 2-4c show that the prepared ink in both the non-continuous and continuous systems could block the flow of a dyed aqueous solution for plotting speeds ranging from 1 to 110%. Only a single pass was needed to effectively contain the sample in the testing region. During the tests, no clogging issue at the tip of the technical pen was experienced that can be partially due to relatively high initial boiling point of Mineral Spirit (145°C to 174°C).

To evaluate the geometrical performance of the continuous flow pen system, the deflection of the plotted circles was measured (Figure 2-4d). The accuracy was calculated from 550 plotted circles: the trueness was -0.2 mm in the X-direction and 0.1 mm in the Y-direction and the precision (95% confidence ellipse) was 0.5 mm in the X-direction and 0.3 mm in the Y-direction. These values are similar to those obtained with the permanent marker system. The coefficients of variation for the inner and outer radii (i.e. the roundness of the plotted circle) were 29% and 9%, respectively, which is similar to that,

obtained using the marker. Further, the coefficient of variation in the line thickness of the plotted patterns (Figure 2-4e) was 32%, which indicates greater consistency than with the marker.

To demonstrate the throughput of the proposed continuous system, 550 circles were plotted with 4 mm diameter at 50% plotting speed with a single pass. To test the water resistance of the circles, the dyed aqueous solution was used (Figure 2-4f shows a representative group of circles). The results show that about 95% (523 out of 550) of the circles were able to contain the aqueous sample within the testing region. The total time needed to plot 550 circles was about 12 minutes using only a single pen; this time can be further reduced by implementing the multi-pen holder (Figure 2-4b).

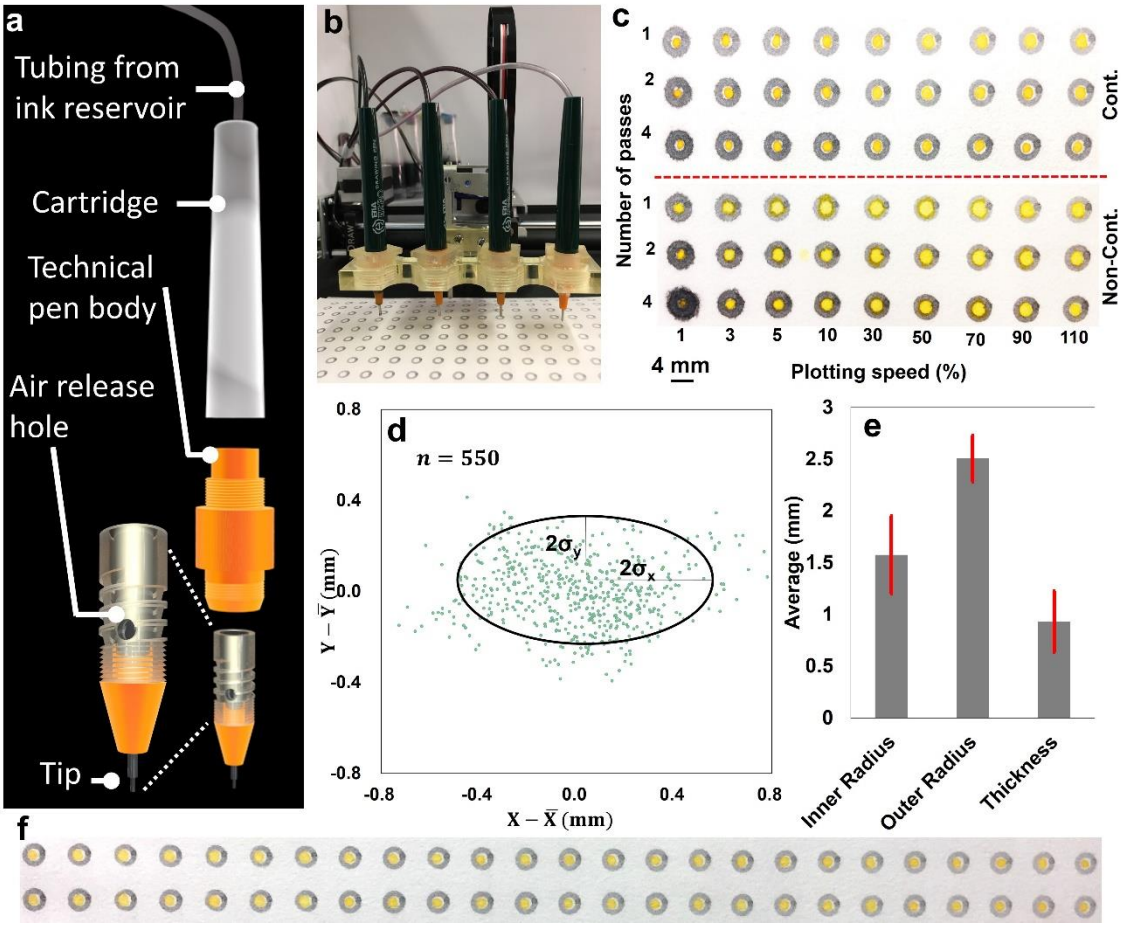

Figure 2-4. Ability of the continuous plotting system in high-throughput fabrication of paper-based microfluidics. *(a) Illustration of continuous ink technical pen. The technical pen was modified by (i) sealing the air release hole of the technical pen, and (ii) creating a hole at the top surface of the cartridge using a hand drill. (b) Technical pens fed continuously by ink. (c) Effect of different plotting speeds and number of passes on water resistance of patterns in continuous (upper) and non-continuous (bottom) plotting system. (d) Deflection of the plotted patterns in both X- and Y-directions (n=550). σx, σy are the total standard deviation in X- and Y-direction, respectively.* $\bar{X}$ *and* $\bar{Y}$ *are the mean deflection in X- and Y-direction, respectively. (e) The mean and standard deviation of inner and outer radius as well as thickness of the plotted patterns with 50% plotting speed (n=550). (f) A representative image shows the ability of the continuous plotting system in high-throughput fabrication of paper-based microfluidics.*

Colorimetric biological assay

To verify the applicability of the proposed fabrication method, colorimetric biological assays were conducted which are useful for clinical urine analysis: nitrite, urobilinogen, protein, blood, and pH assays[10,63,64]. The color formation of various colorimetric reagent solutions was measured as a function of the analyte concentration (for blood, different

numbers of cells per milliliter were used) (Figure 2-5a-d). The color increased as the analyte concentration increased in each assay, as previously reported[16,35,65]. To investigate the ability to measure pH, buffers with different pH values ranging from 5 to 9 (Figure 2-5e) were used. The observed color change was consistent with that which was previously reported[16,35,65]. The results show that the hydrophobic barriers were sufficient to contain the colorimetric reagents and the sample during the reaction so that the color change can be observed.

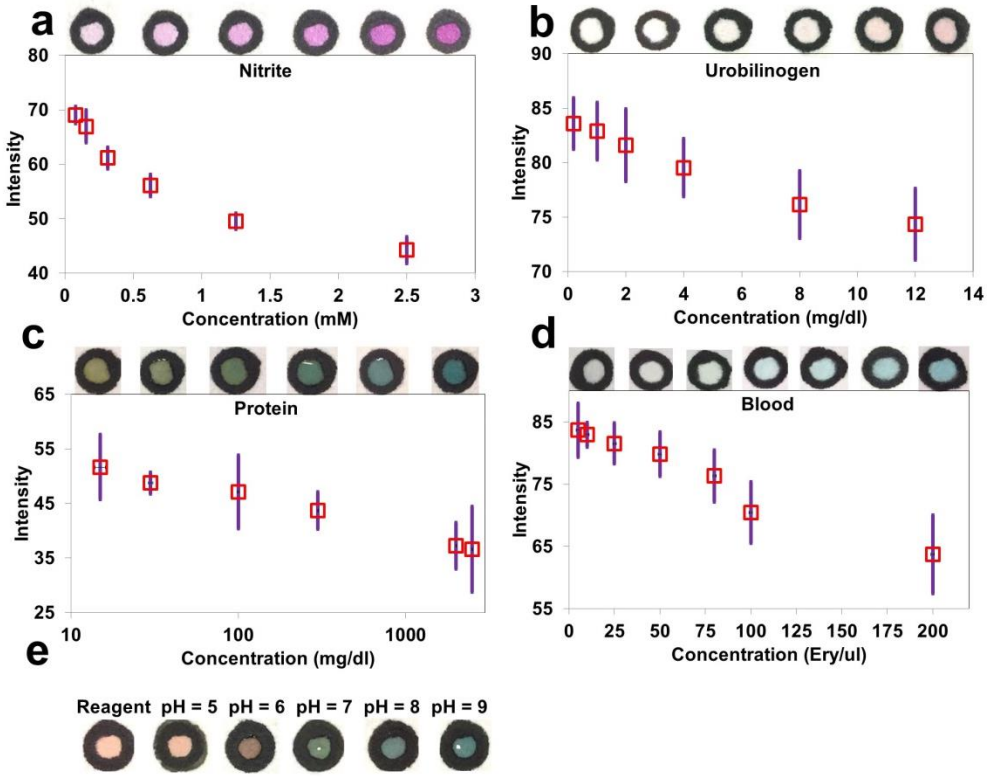

Figure 2-5. Chemical and biological assays via calorimetric method. *The quantified results of the effect of* ***(a)*** *nitrite,* ***(b)*** *urobilinogen,* ***(c)*** *protein (BSA) and* ***(d)*** *blood concentration on color intensities.* ***(e)*** *Effect of pH of solution on color intensity.*

Conclusion

Consider the need for a cost-effective, high-throughput fabrication method for paper-based micro-analytical diagnostic devices, a method was proposed using a pen plotter and hydrophobic marker. In this method, the pen plotter deposits a hydrophobic solution onto a hydrophilic paper to delineate the reaction area where the reagents are contained and the sample is applied. To increase the throughput and decrease the time and cost needed for fabrication of paper-based microfluidics, a custom-designed, low-cost multi-pen holder was used to enable multiplexing of the patterning process with up to eight printing heads. Multiple markers were simultaneously utilized which dramatically decreased the fabrication time. Another improvement for the throughput of the fabrication method was developing a continuous ink supply system. Patterning of 550 circular regions was demonstrated in ~12 min (and can be future reduced to ~3 min using multiple pens) with an estimated cost of less than $1. Testing the water resistance of 550 circular regions shows 95% fabrication success.

Furthermore, to increase the durability, stability and mechanical strength of the fabricated microfluidic devices, the papers were laminated with hot- and cold-laminating layers. Using laminated papers in the fabrication of paper-based microfluidic devices was shown to not only improve their physical properties, but also make handling the devices much simpler. To demonstrate the potential bio-chemical analytical capabilities of the fabrication method, five colorimetric biological assays were conducted: nitrite, urobilinogen, protein, blood, and pH. The novel method proposed here offers low cost, rapid, and simple fabrication of high-resolution paper-based microfluidic devices, which

can be useful for mass production of paper-based microfluidics in both resource-limited and developed countries.

3. CHAPTER 3: Large-scale Fabrication of Paper-based Devices Electrochemical Assays

Introduction

In the development and evaluation of point-of-care devices, the World Health Organization (WHO) established a set of criteria that are collectively referred to as ASSURED: Affordable, Sensitive, Specific, User-friendly, Rapid and robust, Equipment-free, and Deliverable to end-users[66]. Existing medical diagnostic technologies do not fulfill the needs of remote and resource-limited regions due to their complicated clinical infrastructure, long turnaround time, and relatively high costs; thus, new medical diagnostic technologies must be developed[67]. Paper-based assays are promising tools in that they are widely accessible, can be easily produced at high-throughput, and are disposable, and cost-effectiveness[6,8,20,67,68]. To create paper-based assays for a variety of applications, it is necessary to implement various detection methods. Colorimetric detection is one of the most widely used methods and recent studies have developed novel methods to address the inhomogeneity of color[69] and to obtain quantitative measurements[70]. However, the electrochemical detection (ECD) method has also attracted much attention as it is sensitive, inexpensive, portable, and can be miniaturized. Unlike the colorimetric method, ECD can function with impure samples and is not sensitive to changes in the ambient illumination[6,8,20,67,68,69,70,71]. Moreover, ECD requires only simple instrumentation and a small amount of electrical power, making it compatible with use in the field[72]. However, the remaining hurdle to the widespread implementation of paper-based technologies in developing countries is the development of a simple, high-throughput, and low-cost fabrication method[71].

Paper-based devices for electrochemical assays are composed of electrodes and a paper substrate[72,73]. Different methods have been developed for plotting electrodes on paper

such as sputtering[74], sintering[75], inkjet printing[76,77], screen printing[72,78], and direct plotting with a conductive pen or pencil[71,79,80]. For example, Ghosale et al. proposed a method for writing electrodes using a ball-point pen filled with silver nanoparticles capped with octylamine[81]. In another study, Ruecha et al used an inkjet printer to fabricate entire paper-based potentiometric devices including electrodes[77].

Here a low-cost, high-throughput, single-step fabrication method was propose based on a desktop pen plotter integrated with a liquid dispenser. Permanent markers and carbon paste were used to plot the hydrophobic barriers and the electrodes, respectively. A syringe was filled with carbon paste and was connected to a liquid dispenser and the paste flow was driven by the application of a fixed air pressure (Figure 3-1). The paper was hot-laminated on one side to improve its durability, stability, and mechanical strength and provide stability to the hydrophobic barriers and bio-chemical reagents during storage[20].

The electrochemical operation of the fabricated paper-based assays was validated by both cyclic voltammetry (CV) and chronoamperometry (CA) with potassium ferricyanide. Additionally, CA analysis of glucose was conducted to demonstrate a possible diagnostic application of the fabricated paper-based devices for electrochemical assays.

Cyclic voltammetry is of the most widely used techniques for obtaining qualitative information about electrochemical reactions. It linearly scans the potential of a stationary working electrode using a triangular potential waveform. During the potential sweep, the potentiostat measures the current resulting from the applied potential. Chronoamperometry is another technique for electrochemical analysis which measures the current response to an applied potential. It involves stepping the potential of the

working electrodes from a value at which no reaction occurs to a potential at which the surface concentration of the electroactive species is effectively zero. Since the solution is unstirred and working electrode is stationary, a mass transfer is solely by diffusion and the current-time curves reflects the change in the concentration gradient in the vicinity of the surface. This involves a gradual expansion of the diffusion layer associated with depletion of the reactant, and hence decreased slope of the concentration profile as time progresses. Accordingly, the current decays with time[82].

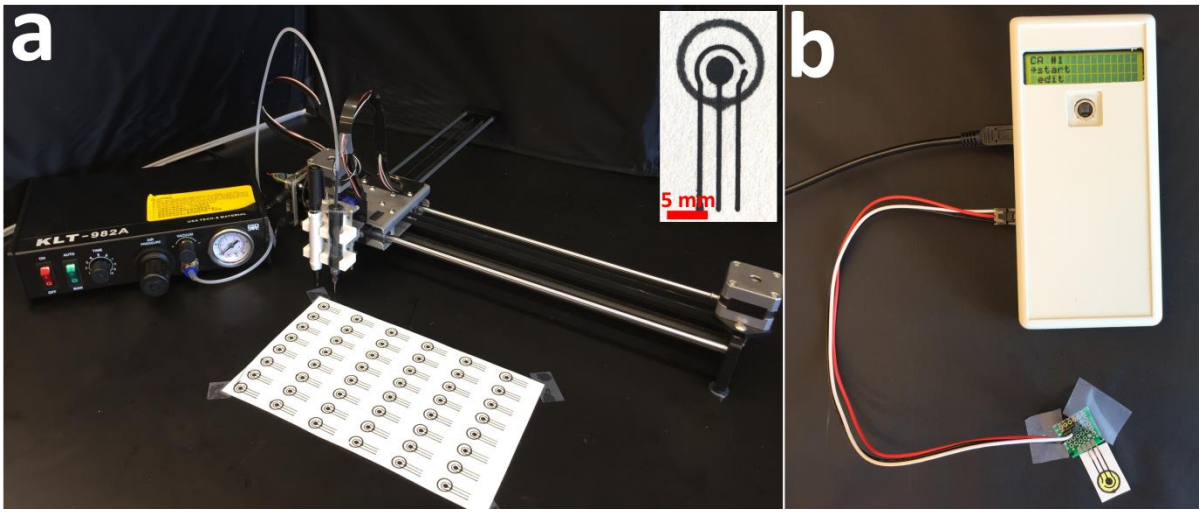

Figure 3-1. Fabrication setup for the paper-based electrochemical devices*. a) Desktop pen plotter integrated with a syringe holder. Also depicted is the liquid dispenser controller used to drive the flow of the carbon ink from the syringe. The inset shows the fabricated paper-based devices for electrochemical assays with three carbon electrodes (working, counter, and reference) and a hydrophobic barrier patterned by a Comix marker. b) Hand-held potentiostat used for cyclic voltammetry (CV) and chronoamperometry (CA) analyses. The potentiostat is connected to one of the fabricated paper-based devices.*

Materials and Methods

Materials

Desktop pen plotter, (AxiDraw) from Evil Mad Scientist Laboratories, CA, US; Double-tipped marker (Comix) from Comix Group Co. Ltd., Shenzhen, China (the fine- and broad-

tips are 0.5 and 2.0 mm in diameter, respectively); Chromatography paper (Whatman No. 1) from GE Healthcare Life Sciences, IL, US; Replicator desktop 3D printer (MakerBot) from MakerBot Industries, NY, US; Hot-laminating layer (GBC EZUse thermal laminating pouches) from Swingline, IL, US; Benchtop laminator (GBC Inspire) from Swingline, IL, US; Potentiostat (Cheapstat) from IO Rodeo Inc, CA, USA; Liquid Dispenser from Advance Electrical Equipment Co. Ltd., Taiwan; Potassium ferricyanide (III) ($K_3[Fe(CN)_6]$, 702587), glucose oxidase (G7141), and potassium chloride (746436) from Sigma-Aldrich, MO, US; Pure glucose from Modernist Pantry LLC., NH, US; Phosphate Buffered Saline (PBS, pH 7.4) from Fisher Scientific, MA, US; Carbon paste from Bare Conductive, London, UK; Screen-Printed Carbon Electrode, (DRP 110) from Metrohm AG, Herisau, China.

Methods

Device Fabrication

To enable a simple, one-step fabrication, a liquid-dispensing plotter was created by integrating a liquid dispenser with an Axidraw pen plotter. A holder was designed in SolidWorks 2016 (Dassault Systèmes SolidWorks Corp., France) to attach the syringe filled with carbon paste to Axidraw and 3D printed it with a Makerbot Replicator. The driver software of the AxiDraw plotter was modified to add another output that can be used to control a liquid dispenser in synchrony with the motion of the pen. The amount of carbon paste deposited was controlled by adjusting the air pressure of the liquid- dispensing controller and the speed of the plotter and, once the desired flow rate is achieved, the pressure was held constant. Using the fine tip of a Comix marker, a 10 mm-diameter circle was plotted on paper as the hydrophobic barrier of the detection zone. Then, the pattern

for the three electrodes (working, counter, and reference) was designed in Inkscape (Free Software Foundation, Inc., MA, US) and plotted with the carbon paste. After plotting the electrodes, the paper was passed through the hot laminator several times to set the carbon paste. Then, a laminating layer was applied to the side opposite the plotted patterns by hot lamination.

Electrochemical measurements

The electrochemical operation of the fabricated devices was validated using potassium ferricyanide (III) ($K_3[Fe(CN)_6]$) and glucose. The electrochemical measurements (CV and CA analyses) were carried out using a potentiostat at the room temperature. CA and CV analyses of $K_3[Fe(CN)_6]$ were carried out at different scan rates (for CV) and step voltages (for CA). The $K_3[Fe(CN)_6]$ samples were prepared by dissolving various amounts of $K_3[Fe(CN)_6]$ in a 1 M-potassium chloride (KCl) solution (the supporting electrolyte). CA analyses were performed on devices on which 50 µl of the $K_3[Fe(CN)_6]$ sample was deposited in the detection zone and on those which were submerged in the same sample. For the glucose tests, the devices were prepared by depositing 10 µl of a solution of 300 U/ml glucose oxidase and 20 mM $K_3[Fe(CN)_6]$ (the mediator) in PBS in the detection zone and drying at room temperature for 10 min. The CA analysis was then conducted by depositing 50 µl of a glucose sample dissolved in DI water. The mechanism for glucose detection involves glucose oxidation by the catalyst activity of glucose oxidase, leading to the reduction of $Fe\ (III)$ to $Fe\ (IV)$ and the generation of $Fe(CN)_6^{4-}$ ions, which are detected by the electrochemical analysis (Equations 1-3)[83].

$$glucose + 2K_3[Fe(CN)_6] + H_2O \xrightarrow{glucose\ oxidase} gluconic\ acid + 2K_4[Fe(CN)_6] \quad (1)$$

$$2Fe(CN)_6^{4-} \xrightarrow{anodic\ electrode} 2Fe(CN)_6^{3-} + 2e^- \quad (2)$$

$$2Fe(CN)_6^{3-} + 2e^- \xrightarrow{cathodic\ electrode} 2Fe(CN)_6^{4-} \quad (3)$$

To compare the performance of the fabricated devices with the performance of commercially-available screen-printed electrodes (SPEs), CA analyses were performed with different concentrations of $K_3[Fe(CN)_6]$ and glucose. Unlike the devices fabricated by the proposed method, the electrodes in the SPEs were screen-printed with silver/silver chloride (Ag/AgCl) and the portions of the working and counter electrodes in contact with samples were covered by screen-printed carbon. However, we were not able to immobilize the glucose reagents on the ceramic surfaces of the SPEs. Thus, 10 µl of glucose oxidase and $K_3[Fe(CN)_6]$ solution was dried on a 6×8 mm piece of chromatography paper at room temperature. The paper was placed on the detection zone of the SPE, 50 µl of the glucose sample was deposited on this paper, and CA analyses were carried out by applying a 300-mV potential.

Results and Discussion

The electrochemical behavior of the fabricated paper-based devices was validated by CV and CA with a model electroactive compound, $K_3[Fe(CN)_6]$ in 1 M KCl at various scan rates between 50 and 500 mV/s. The CV results (Figure 3-2a) showed that as the scan rate was increased, the peak current (the anodic, I_p, and cathodic, I_{-p}, peak currents) increased and that relationship is consistent with the Randles-Sevcik equation. The peak current for a reversible couple (at 25 °C) given by Randles-Sevcik equation is as follow:

$$I_p = (2.69 \times 10^5) n^{3/2} A C D^{1/2} \nu^{1/2} \quad (4)$$

Where *n* is the number of electrons, *A* is electrode area, *C* is the concentration, *D* is the diffusion coefficient, and ν is the scan rate. Accordingly, the current is directly proportional to concentration and increases with square root of the scan rate.

The I_p/I_{-p} ratio was close to unity for all of scan rates tested and the peak shapes matched the characteristic graph of a typical reversible (Nernstian) electrochemical reaction [20]. It should be noted that for fast reversible reactions that transfer one electron, including the redox-active couple of $Fe(CN)_6^{3-}/Fe(CN)_6^{4-}$, the voltage separation (voltages at which the peaks occur) should theoretically be only 59 mV and independent of the scan rate[84]. However, due to the strong effect of the carbon paste composition on the electrode reactivity, electron-transfer rates can be decreased[82] and lead to the increase in the voltage separation from 120 to 320 mV by increasing the scan rates from 50 to 500 mV/s. This observed discrepancy generally occurs when the Nernstian equilibrium cannot be maintained over the course of the reaction, causing the current peaks to occur at voltages that are farther apart as the scan rate is increased. Moreover, the results show that the difference between the voltages at which the peak occur depends on the scan rate. This also indicate that the electron transfer kinetics was slow since the voltages at which the peak currents occur at all scan rates is characteristic of the electrode reaction[84].

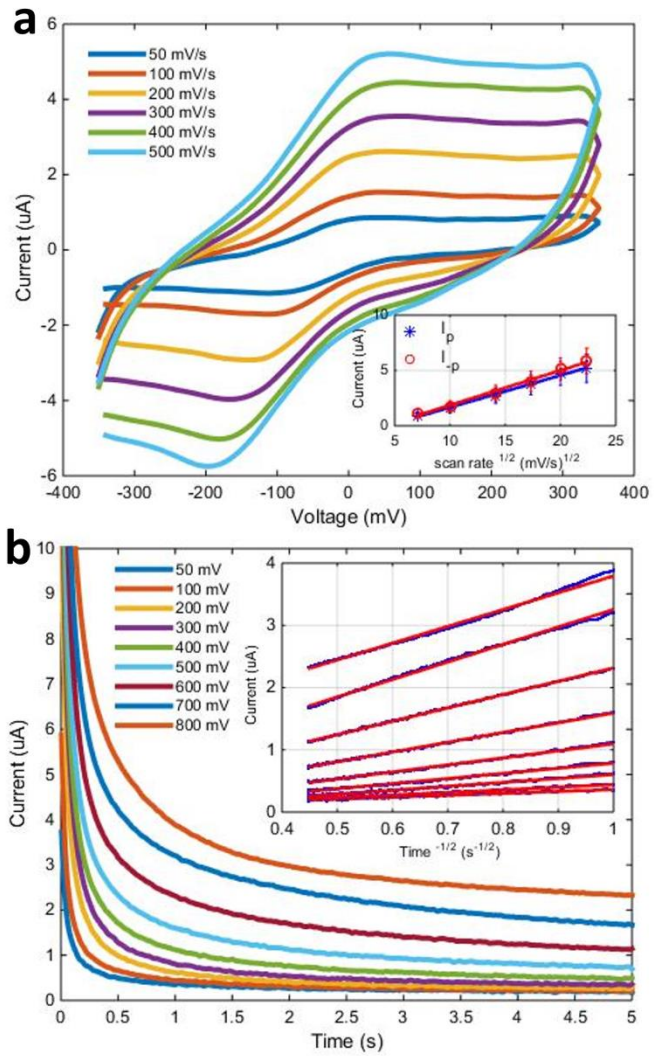

Figure 3-2. Electrochemical characterization of the paper-based devices for electrochemical assays*. a) Cyclic voltammetry results for 5 mM $K_3[Fe(CN)_6]$ in 1 M KCl obtained at different scan rates: 50, 100, 200, 300, 400, and 500 mV/s. The inset shows the anodic (I_p) and cathodic (I_{-p}) peak currents versus the square root of the scan rate and the solid line represents a linear fit to this data with the equation y = 0.28938x - 1.2309 (R^2 = 0.99529) and y = 0.31432x - 1.279 (R^2 = 0.99118), respectively; (n = 10). b) Chronoamperometry result for 5 mM $K_3[Fe(CN)_6]$ in 1 M KCl at different step voltages: 50, 100, 200, 300, 400, 500, 600, 700, and 800 mV. The inset shows the current versus the negative square root of time with the solid line representing linear fits to this data; (n = 10).*

CA was also tested because it is more compatible with long-term use[72] and has a higher signal-to-noise ratio[83]. CA analysis was performed on the same model electroactive compound (5 mM $K_3[Fe(CN)_6]$ in 1 M KCl) at different step voltages between 50 and 800 mV. The result (Figure 3-2b) shows that the current increased as the step voltage

increased. In addition, the current decay was proportional to the concentration and $t^{-1/2}$, which is consistent with the Cottrell equation $I = nFAC\sqrt{D}/\sqrt{\pi t}$, where *I* is the current, *n* is the number of electrons released from each molecule, *F* is the faraday constant, *A* is the surface area of the working electrode, *C* is concentration of the electroactive compound and *D* is the diffusion constant.

CA analysis was conducted on different concentrations of $K_3[Fe(CN)_6]$ using both the fabricated devices and the SPEs. The results obtained by pipetting the sample onto each of the devices showed that the current increased as the concentration increased (insets of Figure 3-3a, b). Moreover, these results were compared with the results obtained by dipping the fabricated devices. CA results obtained with the fabricated devices by dipping the detection zones into the same samples (Figure 3-3c). Comparing the measurements, it was found that depositing the sample resulted in more consistent results as evidenced by a smaller R-squared value for the linear fit to the concentration-versus-current data while dipping into the sample resulted in a higher standard deviation over repeated measurements and lower current readings.

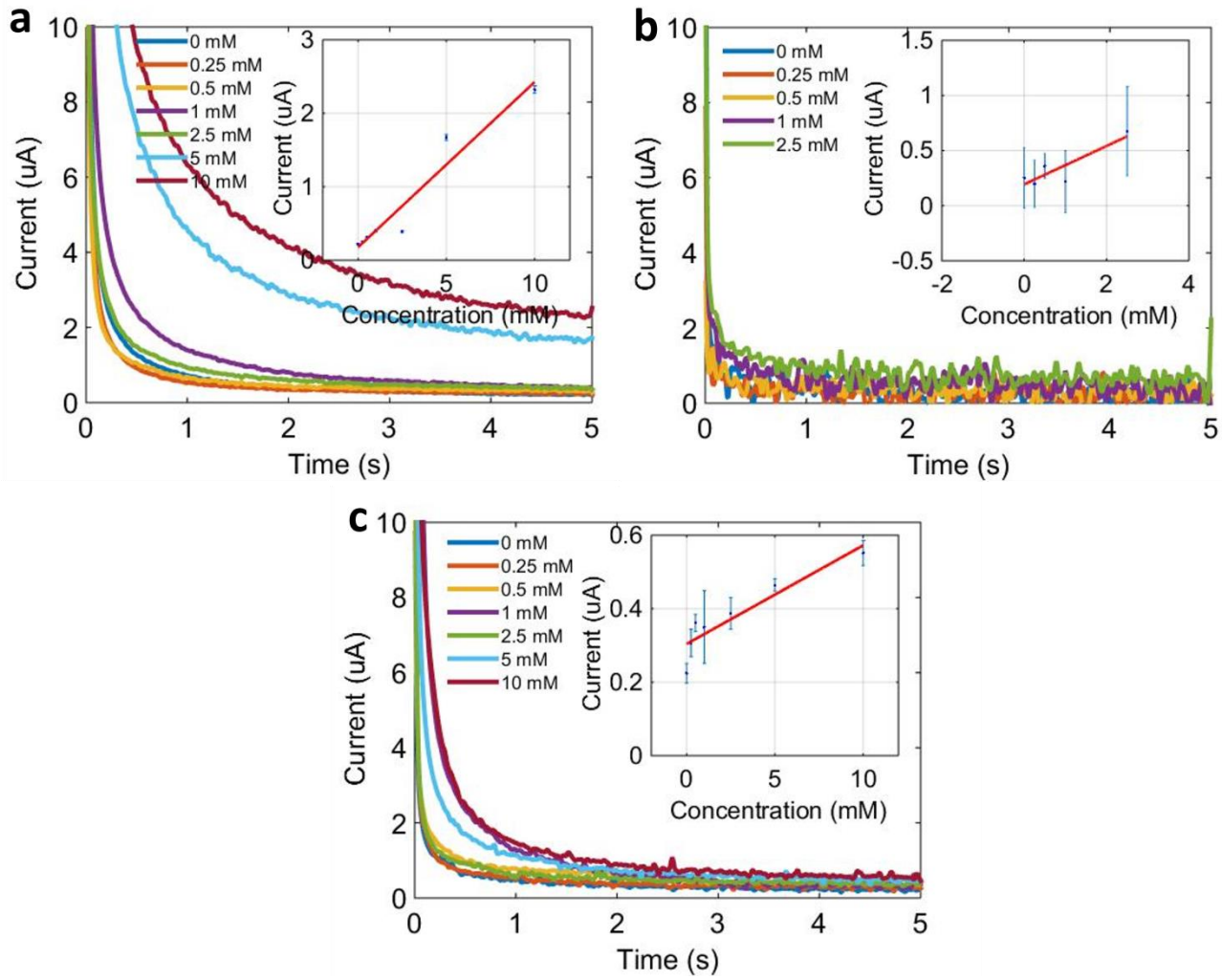

Figure 3-3. Chronoamperometry results for different concentrations of $K_3[Fe(CN)_6]$ in 1 M KCl obtained *by depositing the sample on a) the fabricated paper-based devices and (b) commercial screen-printed electrodes; and c) by dipping the fabricated devices into the sample. The insets show the steady-state currents for the range of concentrations and the solid lines represents linear fit to the data with the following equations: a) y = 0.22484x + 0.17608 (R^2 = 0.93673), b) y = 0.19295x + 0.1699 (R^2 = 0.98655), c) y = 0.026825x + 0.30412 (R^2 = 0.85059), (n=5).*

Finally, the performance of the fabricated devices was tested for a common diagnostic application: glucose testing. A glucose assay was conducted using both the paper-based devices and the SPEs. The effect of the time on the CA results was investigated because the chemical/enzymatic reaction responsible for the electron transfer in the glucose assay requires time to reach to a steady rate. The CA results obtained from the fabricated device

with 5 mM glucose (Figure 3-4a) show that the measured current increased as the time increased. Moreover, the glucose concentration for study was chosen in the range of 0 to 20 mM (Figure 3-4b,c), as it is relevant to the range of glucose concentrations found in urine. The results show the current increased linearly with the glucose concentration in both the fabricated devices and the SPEs although the sensitivity of the SPEs was higher than that of the fabricated devices (Figure 3-4c).

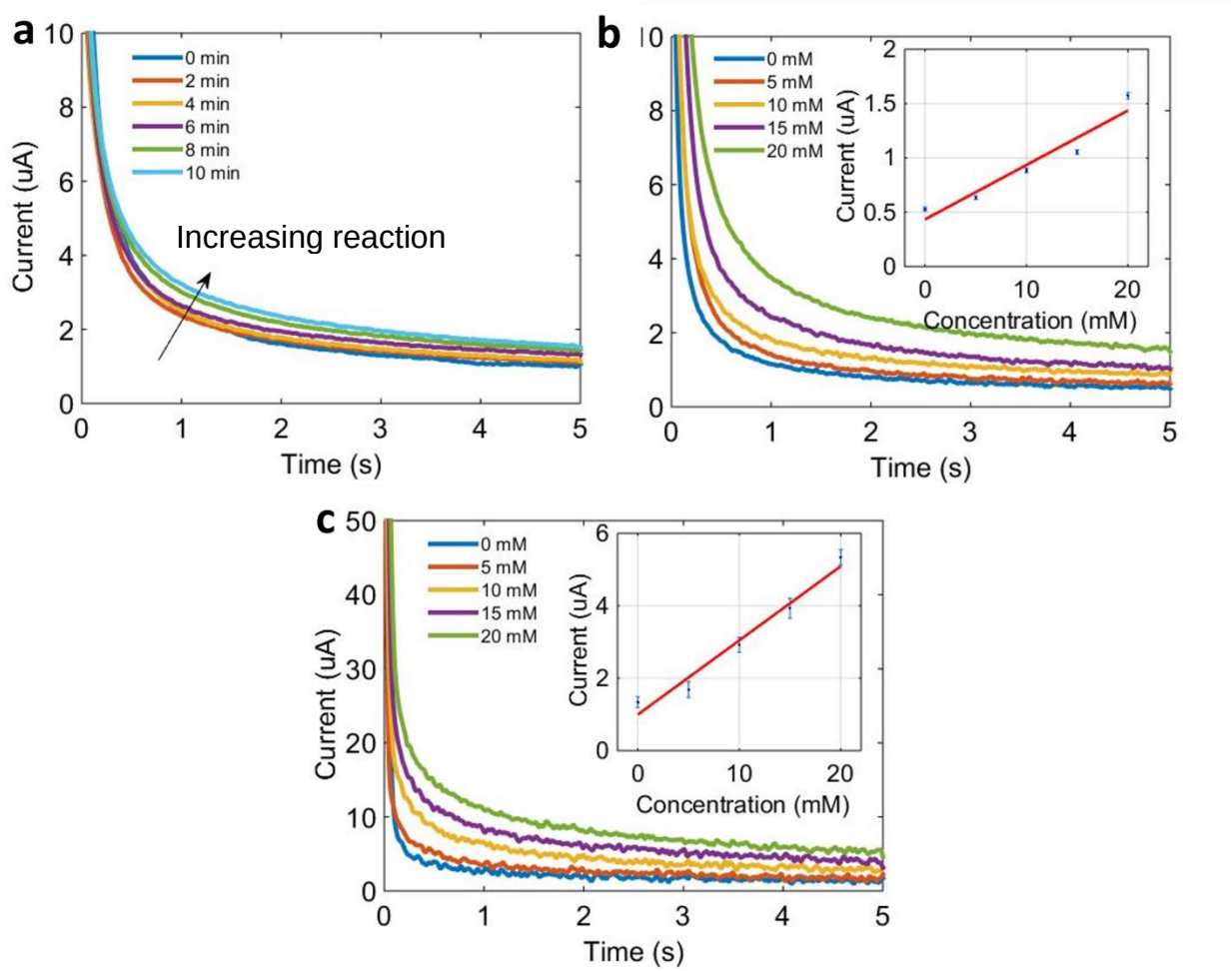

***Figure 3-4. Chronoamperometry results for glucose**. a) Effect of reaction time. Effect of concentration with b) the fabricated paper-based devices and c) the commercial screen-printed electrodes. The insets in the graphs in b) and c) show the steady-state currents for the range of concentrations and the solid lines represents linear fits to the data with the following equations: b) y = 0.0501x + 0.4339 (R^2 = 0.926) and c) y = 0.2047x – 0.9966 (R^2 = 0.969), (n=5).*

Conclusion

In this study, a high-throughput and cost-effective method were presented to fabricate paper-based devices for electrochemical assays. In this method, a liquid dispenser was used to deposit carbon paste in a pattern with a desktop plotter to form the electrodes (working, counter, and reference) required for electrochemical detection of target analytes. This one-step method is both fast and cost-effective: 50 devices can be fabricated in approximately 18 min and each device costs less than 0.02 USD based on the cost of materials. A hand-held potentiostat was used to conduct CV and CA analyses, which demonstrates the applicability of this technique. The fabricated devices were validated for CV and CA using a model electroactive compound, $K_3[Fe(CN)_6]$ in KCl. To validate the potential of the presented method for fabricating diagnostic tools, CA analysis was used to conduct a glucose assay. The experimental results showed a linear increase in the current as a function of the glucose concentration.

4. CHAPTER 4: Measuring Concentration of Electrolytes in Urine Using Miniaturized Paper-based Smartphone-enabled Devices

Introduction

Deviation of inorganic ion concentrations, such as sodium (Na^+), potassium (K^+), calcium (Ca^{2+}), and chloride (Cl^-), from the commonly accepted healthy ranges and the presence of nitrite (NO_2^-) in human body fluids can be a symptom of a disorder or a dysfunction of an organ[85]. If such a malfunction goes undiagnosed and left untreated, it can lead to serious health issues. Regularly monitoring sodium, potassium, and calcium levels in urinary excretion can help to diagnose such disorders as hypertension and cardiovascular diseases, hyperkalemia or hypokalemia (disorders which can be caused by changes in potassium intake), kidney disease or injury, adrenal gland problems, rickets, hypothyroidism, steatorrhea, vitamin D overdose, and renal tubular acidosis[86,87,88,89,90]. Additionally, measuring these cations is useful for people with urinary stone disease since calcium is the main component of urinary stones; urinary sodium and potassium are also related to urinary calcium excretion[91]. Moreover, sodium and potassium intake is commonly analyzed via urine samples[88]. Chloride and nitrite ion measurements are used in the diagnosis of disorders such as cystic fibrosis and diabetic acidosis[92], while nitrite is also used to estimate the probability of a urinary tract infection (UTI) since nitrite is a metabolic product of typical pathogens of the urinary tract[93]. . In healthy urine, nitrite is not present, but rather is produced by bacterial reduction of urinary nitrate[94].

For determining the cation and anion concentrations in urine, different analytical methods are used, including flame emission spectrophotometry[95], ion selective electrodes[96], ion chromatography[97] and capillary electrophoresis[98], all of which are accurate, precise and repeatable. However, the total analysis time, the amount of sample required, and the analysis cost of these methods may be relatively high[85,95,99]. Alternatively, paper-based

devices are cost-effective, provide rapid analysis, and have a wide-range application in many fields, including pharmaceutics[100], food safety[101,102], environmental monitoring[103] and medical diagnostics[6,9,20,104,105]. Dipsticks and lateral flow immunoassays (LFIA) are just two examples of common paper-based diagnostic devices with many real-world applications. Nevertheless, paper-based devices which measure clinically-important analytes are still scarce[105] in the market; there is an unmet need for developing such devices in a high-throughput, low-cost manner.

Regarding the importance of measuring electrolytes in urine, finding a cost-effective, sensitive, and simple-to-use device can be valuable in both resource-limited regions, as well as developed countries. To the best of our knowledge, for the first time in this field, we developed a cost- and time-effective paper-based sensor for measuring the concentration of Na^+, K^+, Ca^{2+}, and Cl^- ions in urine which is easily and accurately quantified using a smartphone-enabled platform. The fluorescent detection method was chosen for detecting Na^+, K^+, and Ca^{2+} ions and the colorimetric method for detecting Cl^- ions. The reagents were immobilized on a paper matrix and deposited the sample, followed by reading the fluorescent intensity and/or color intensity for quantification of the ion concentrations. By testing the device with both Tris buffer and artificial urine containing a wide range of concentrations of the electrolytes, the results show that the proposed device can be used for detecting electrolytes within the whole physiological range of concentrations.

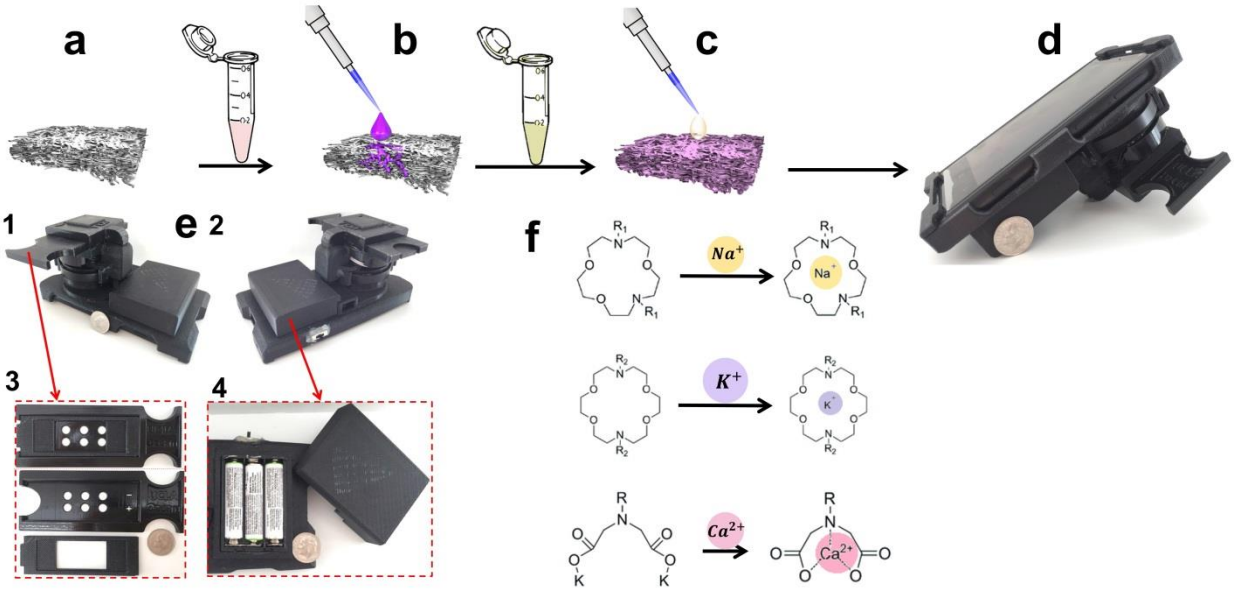

Figure 4-1. Schematic procedure of measuring the concentration of cations*. (a) Chromatography paper cut with laser cutter (Ø = 0.25 in). (b) Depositing 2 µl of fluorescent probe (Sodium green, PBFI, and Fluzin) on paper. (c) Adding the solution that contains the Na^+, K^+, or Ca^{2+} ions. (d) Reading the fluorescent intensity by a smartphone-enabled platform. (e) 1,2. Smartphone-based platform from side view, 3. Sample holder, 4. Backside of the platform. (f) Chelation mechanism of fluorescent probes (from top to bottom: sodium green, PBFI, and Fluozin).*

Material and Methods

Materials and Equipment

Sodium Green (S6900) and Tetraammonium Salt, PBFI (P1265MP), Tripotassium Salt, FluoZin™-1 (F24180); Corning 96-Well Clear Bottom Black Polystyrene Microplate (07-200-565) from Thermo Fisher Scientific Inc., MA, US; Lactic acid (W261106), Citric acid (C0759), Magnesium sulphate (746452), Ammonium chloride (A9434), Calcium chloride (C1016), Potassium chloride (746436), Sodium chloride (S9888), Sodium bicarbonate (792519), Manganese (II) chloride (244586), Tris base (648310), Tris hydrochloride (10812846001), Nickel (II) chloride, Sodium nitrite (237213), Sulfanilamide (S9251N), N-(1-Naphthyl)ethylenediamine (33461), and Chloride assay kit (MAK023) from Sigma, US; Potassium phosphate dibasic (7758114) from Acros Organics, Geel, Belgium; Potassium

dihydrogen phosphate (104873) and Urea (108487) from EMD Milipore Co., MA, US; Dimethyl Sulfoxide, DMSO, (25-950-CQC), Corning Inc., NY, US; Whatman No. 1, GE healthcare life sciences, IL, US; Synergy H1 Hybrid reader, Biotek, VT, US; CO_2 laser-cutter, Universal Laser Systems Inc., AZ, US; Blue LEDs (516-2800-1-ND), Digi-Key Corporation, MN, US; Ultraviolet (UV) LEDs (160-2184CT-ND), Digi-Key Corporation, MN, US; Excitation bandpass filter (ET470/40x), Chroma Inc., VT, US; Long-pass emission thin-film filter (FF01-500/LP-23.3-D), Semrock Inc., NY, US; Thermoplastic 3D printing filament (ABS P430 Plus) and 3D printer (Dimension Elite) from Stratasys Ltd., MN, US;

Methods

To quantify the concentrations of Na^+, K^+, and Ca^{2+} ions, fluorescent probes Sodium Green as the sodium indicator, PBFI potassium-sensitive dye, and Fluozin calcium indicator were chosen. Chromatography paper (Whatman No. 1) was used as the reaction matrix on which the fluorescent probe solutions with concentrations of 25 µM were immobilized. The fluorescent probes were diluted using DMSO since this organic solvent prevents hydrolysis. During the first phase of experiments (Figure 4-1 to 4-5), a microplate reader was used to measure the fluorescence intensities of the probes. To accommodate the microplate reader, the papers were cut into a round shape (Ø = 0.25 in) using a CO_2 laser-cutter. 2 µl of fluorescent probe was deposited on the paper matrix followed by 2 µl of the metal ion solution. The papers were then placed at the bottom of the microwells in 96-well plates for reading the fluorescent intensity of the probes. The excitation/emission peaks were 485 nm/541 nm for detection of sodium and calcium ion and 360 nm/450 nm

for detection of potassium ion. The effect of elapsed time on fluorescent intensity after depositing the ion solution on the paper and before reading the intensity was investigated (Figure 4-2).

Additionally, the sensing selectivity of the sensors in the presence of other ions (including magnesium, manganese, nickel, and ammonium) present in human urine was studied (Figure 4-3). Furthermore, the detection of ions was tested in two different solutions: Tris buffer (150 mM, pH 7.4) and artificial urine (pH 6) (Figure 4-4a-c and Figure 4-5a-c). To quantify Cl^- concentration in DI and artificial urine, 2 µl and 4 µl of the reagent was spotted on paper, respectively. After drying the reagent, 2 µl of sample containing Cl^- ions was deposited on paper. The blue color on the paper was captured using by the camera of an iPhone 6 and the images were processed by a MATLAB script. The results are shown in Figure 4-4d (Cl^- ions in DI) and Figure 4-5d (Cl^- ions in artificial urine). To detect NO_2^- ions, a reagent containing sulfanilamide (50 mM), N-(1-Naphthyl)ethylenediamine (10 mM) and citric acid (330 mM)[106] was used. After depositing 2 µl of reagent on the paper, 2 µl of sample containing different concentrations of nitrite ions was added. The color of the paper changed to pink upon adding the nitrite ion. This color change was captured by the camera of an iPhone 6 and the taken images were processed by a MATLAB script. The quantified results are presented in Figure 4-4e (NO_2^- ions in Tris buffer, 150 mM, pH 7.4) and Figure 4-5e (NO_2^- ions in artificial urine). During the next phase of experiments, the plate reader was replaced with the smartphone-enabled platform and measured the concentration of ions in an artificial urine sample (Figure 4-6).

Preparation of ion solutions

Sodium, potassium, calcium, and nitrite ion solutions in Tris buffer (150 mM, pH 7.4) and chloride ion in DI were prepared using sodium chloride, potassium chloride, calcium chloride, sodium nitrite, and sodium chloride respectively. The stock solutions were serially diluted to the desired concentrations of sodium (0.25-250 mM), potassium (0.25-250 mM), calcium (0.25-10 mM), chloride (10-300 mM) and nitrite (0.1-2 mM) ions.

To investigate the selectivity of the fluorescent probes for detecting cations, different ion solutions were prepared at four concentrations including 1, 10, 100 mM, and a physiological concentration. For the physiological concentration, the maximum ion concentration found in human urine was considered, as follows: sodium (220 mM), potassium (125 mM), calcium (10 mM), magnesium (15 mM), manganese (1 mM), nickel (1 mM) and ammonium (70 mM). Sodium chloride, potassium chloride, calcium chloride, magnesium sulfate, manganese (II) chloride, nickel (II) chloride, and ammonium chloride were used for preparing these solutions, respectively. To investigate the selectivity of each fluorescent probe, 2 µl of different ion solutions were deposited on the paper after depositing 2 µl of the fluorescent probe solution. By reading the fluorescent intensity in the presence of each of the ions, the results were compared. The selectivity of the fluorescent probes was determined based on the intensity of each fluorescent probes in the presence of ions in the solution.

Preparation of artificial urine and standard solutions

The artificial urine solution was prepared as reported by Martinez et al[107]. This solution contained 1.1 mM lactic acid, 2.0 mM citric acid, 25 mM sodium bicarbonate, 170 mM

urea, 2.5 mM calcium chloride, 100 mM sodium chloride, 2.0 mM magnesium sulfate, 10 mM sodium sulfate, 7.0 mM potassium dihydrogen phosphate, 7.0 mM dipotassium hydrogen phosphate, and 25 mM ammonium chloride dissolved in DI water. The pH of the solution was adjusted to 6 using 37% hydrochloric acid. To prepare artificial urine solutions containing different concentrations of sodium, potassium and chloride ions, sodium bicarbonate and sodium chloride with a molar ratio of 4, potassium dihydrogen phosphate and dipotassium hydrogen phosphate with a molar ratio of 1, and calcium chloride, ammonium chloride, and sodium chloride with a molar ratio of (1: 10: 40) were used, respectively.

Design and fabrication of smartphone-enabled microscope

A cost-effective mobile fluorescence microscope was developed, which consisted of a 3D-printed housing which aligns with the camera of the smartphone, an external lens, an excitation filter, an emission filter, a light emitting- diode (LED), a sample tray, and three batteries (Figure 4-1e). A Nokia Lumia 1020 was used in the design of the smartphone-enabled fluorescence microscope and were able to capture 38MP raw format (i.e. digital negative (DNG)) images at a 4:3 aspect ratio. The image sensor has a pixel size of 1.12 µm and the built-in objective lens of the cellphone has a focal length (f) of 7.2 mm and a relative aperture of f/2.2. Furthermore, through the built-in camera settings, we were able to adjust a variety of camera parameters (i.e. white balance, focus, ISO speed, exposure time, and contrast) to capture optimal images. Eight blue LEDs were used to excite the fluorescent probes conjugated to sodium and calcium ions and an ultraviolet (UV) LED for potassium ion measurements. The lights were powered by three AAA alkaline

batteries. The emission spectrum of the LEDs was filtered using an excitation bandpass filter with a wavelength of 470 nm and bandwidth of 40 nm. An aspherized achromatic lens with a focal length f = 30 mm was used to create a magnification factor of 0.24 (i.e. f/f2) between the sample plane and the CMOS sensor of the mobile-phone, which helped us achieve a large sample FOV (~1 cm^2) per image without any mechanical scanning. To adjust the depth of focus of the microscope, a z-stage was placed between the external lens and the excitation source. To block the excitation light, a long-pass emission thin-film filter with a cut-off wavelength of 515 nm was placed between the cell phone lens and the external lens. The custom-designed optomechanical housing of the fluorescence microscope attachment was also 3D-printed using ABS thermoplastic material.

After capturing the fluorescence image, a custom-designed smartphone application wirelessly transmits the image to a server at UCLA for rapid and automated quantification of the ion concentrations. The images are processed using the custom-developed algorithms and the concentration result of each ion in the sample of interest is returned back to the smartphone within ~90 s, and is displayed to the user through the smartphone application. This smartphone-based, field-portable fluorescent microscopy platform, together with the digital image processing framework, can provide a valuable solution for automated and rapid determination of ion concentrations, even in remote and resource-limited settings.

Results and Discussion

Effect of elapsed time on fluorescent intensity of probes

Na^+, K^+, and Ca^{2+} ions were detected in Tris buffer solution (150 mM, pH 7.4) at different concentrations at room temperature and investigated the effect of elapsed time on the

intensity of fluorescent probes during a 3-hour interval. Figure 4-2 shows that the intensity of the fluorescent probe for detecting Na^+ did not change significantly over time. On the other hand, the intensity of the fluorescent probe for detecting K^+ decreased gradually with passing time until after approximately 2 hours when it became almost constant. The intensity of the fluorescent probe for detecting Ca^{2+} became constant after approximately 150 minutes.

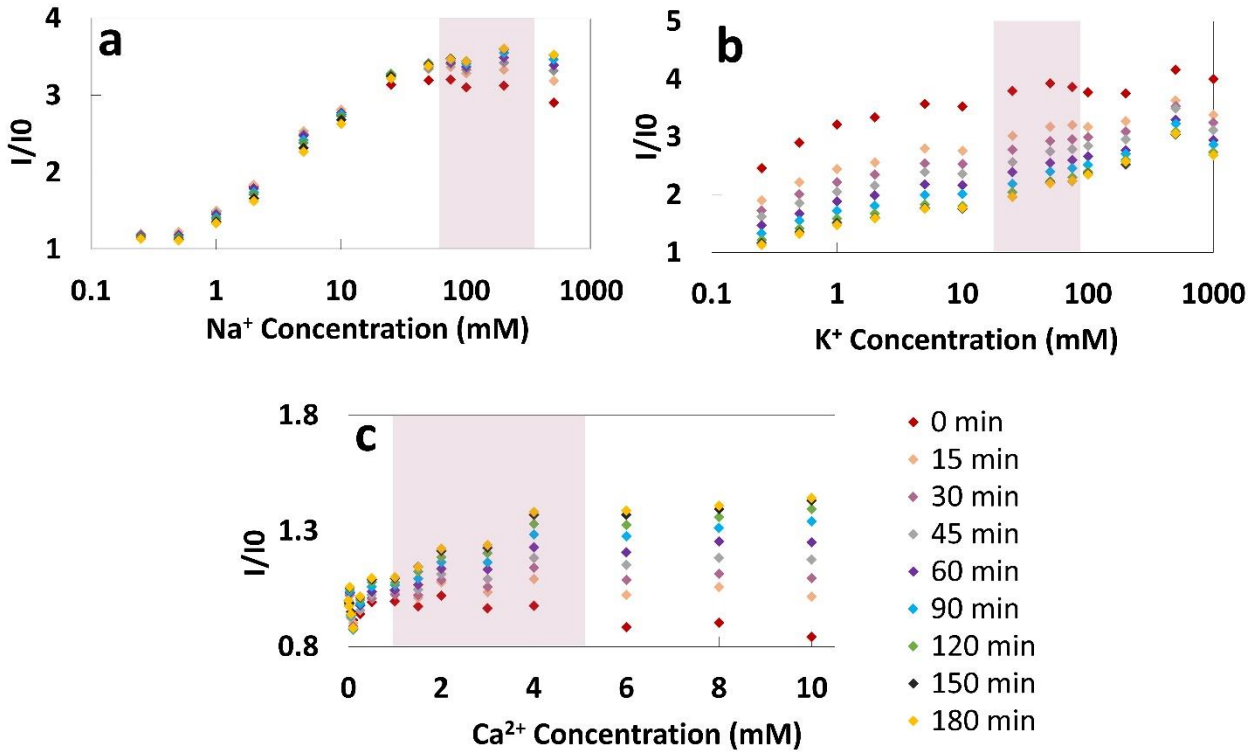

Figure 4-2. Investigating the effect of elapsed time on fluorescent intensity of probes *for (a) Na^+, (b) K^+ and (c) Ca^{2+} ions for a range of concentrations. Elapsed time refers to the time passed between depositing the ion solution on the paper and reading the intensity: elapsed time was varied from 0 to 3 hours.*

Selectivity of fluorescent probes

Urine is comprised of mostly water, but it contains other substances, including ions of various concentrations. Magnesium (Mg^{2+}), manganese (Mn^{2+}), nickel (Ni^{2+}) and ammonium (NH_4^+) are some of the most common ions in urine, in addition to sodium,

potassium, and calcium ions. The selectivity of the sodium, potassium, and calcium fluorescent probes (sodium green, PBFI and Fluozin, respectively) was studied in presence of Mg^{2+}, Mn^{2+}, Ni^{2+}, and NH_4^+ ions. Figure 4-3a shows that for all concentrations (1, 10 and 100 mM) of the above ions, the fluorescent probes performed as expected: sodium green had the highest fluorescent intensity in presence of Na^+, PBFI had the highest fluorescent intensity in presence of K^+, and Fluozin had the highest fluorescent intensity in presence of Ca^{2+}.

To simulate conditions close to those of a real urine sample, the maximum physiological concentration of each ion in urine was considered and the extent of interference was investigated. Sodium Green had the highest fluorescent intensity in the presence of Na^+ (1.88- and 2.41-fold higher than that in the presence of K^+ and Ca^{2+} ions, respectively). Moreover, PBFI showed the highest intensity in the presence of K^+ (1.55- and 2.4-fold higher intensity than that in the presence of Na^+ and Ca^{2+} ions, respectively). Similarly, Fluozin showed the highest intensity in the presence of Ca^{2+} (1.77-, 1.59-, and 1.52-fold higher intensity than that in the presence of Mg^{2+}, Mn^{2+} and Ni^{2+} ions).

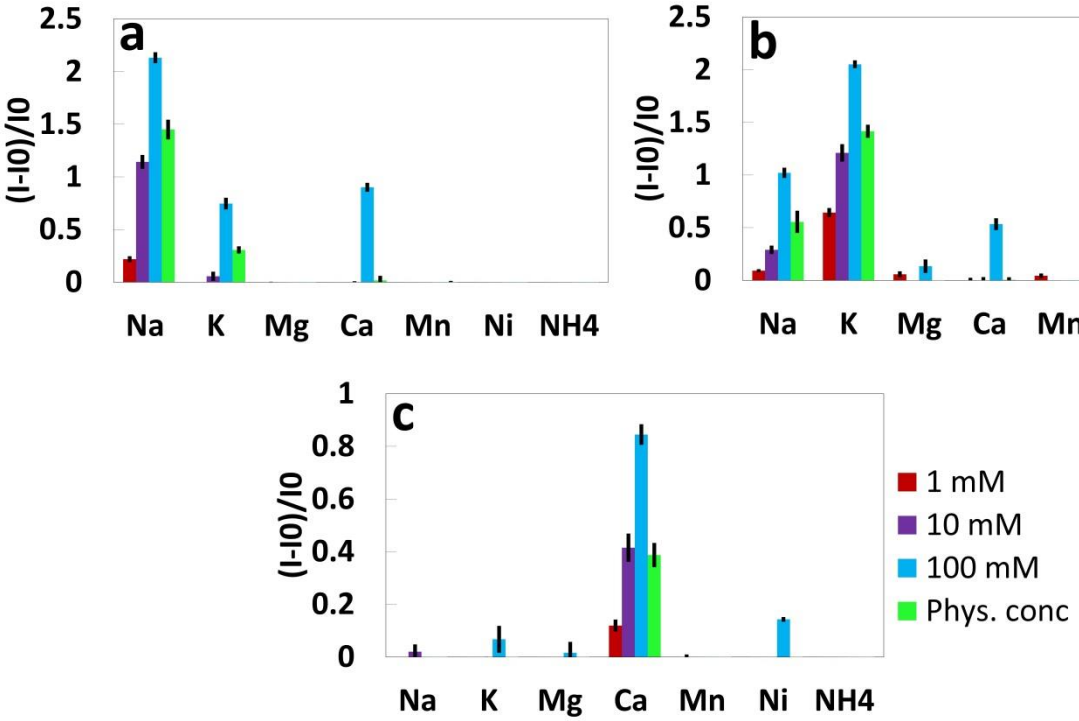

Figure 4-3. Selectivity of fluorescent probes. *Selectivity of 25 µM (a) Sodium green, (b) PBFI, and (c) Fluzin towards different ions in Tris buffer solution (150 mM, pH 7.4) at concentrations of 1, 10, 100 mM, and their maximum physiological concentration. Excitation/Emission wavelength of Sodium Green ($\lambda_{ex}/\lambda_{em}$: 485/541 nm), PBFI ($\lambda_{ex}/\lambda_{em}$: 360/450 nm), and Fluzin ($\lambda_{ex}/\lambda_{em}$: 485/541 nm). Error bars represent the standard error of the mean (n=6).*

Effect of the concentration of the electrolytes on intensity

The concentration of Na^+, K^+, Ca^{2+}, and Cl^- in healthy urine is in the range of 100-260 mmol/day (65-175 mM), 25-100 mmol/day (15-70 mM), 2.5-7.5 mmol/day (1.5-5 mM), and 80-250 mmol/day (50-170 mM), respectively, while healthy urine should not contain any nitrite ion[108]. It should be noted that since the volume of urination per day varies between 0.8 and 2 liters, an average volume of 1.5 liters was considered for calculating the physiological concentration range of ions in mM. To cover the whole physiological range of urinary ion concentrations, solutions with a wide range of concentrations were prepared. It can be seen in Figure 4-4a-c that the fluorescent intensity of probes increased with increasing concentration of ions in Tris buffer (150 mM, pH 7.4). The fluorescent

intensity of the sodium and potassium fluorescent probes increased 351.9% and 304.3% by increasing the Na^+ and K^+ ion concentrations from zero to 500 mM, respectively. By increasing the concentration of Ca^{2+} in the buffer solution from zero to 10 mM, the intensity of the probe increased 143%. The fluorescent intensity ratio as a function of concentration can be expressed as

$$\frac{I}{I_0} = A - Be^{-\propto C} \quad (1)$$

where I and I_0 are the intensities of the solution with and without ions, respectively, $\propto$ is the saturation decay constant, C is the ion concentration in the solution, and A and B are constants[109].

The saturation decay constant for Na^+, K^+, and Ca^{2+} ions in Tris buffer solution (150 mM, pH 7.4) and their R-squared values are summarized in Table 4-1. The high R-squared values obtained from the exponential curve fitting (Eq. 1) to the experimental data is representative of good agreement between the experimental results and theory. The results showed that at low ion concentrations, the intensity ratio was linearly proportional to the ion concentrations; this linearity occurred in the concentration range of 0-5 mM (R-squared 0.922), 0-1 mM (R-squared 0.958), and 0-4 mM (R-squared 0.955) for Na^+, K^+, and Ca^{2+} ions in Tris buffer (150 mM, pH 7.4), respectively. By increasing the concentration of ions, a deviation from linearity occurred which could be due to the absorbing the emitted signals by the ions in solution[110].

Table 4-1. Calibration parameters and Limit of Detection (LOD) of sodium, potassium and calcium ions

Media	Ion	Calibration curve				Exponential Equation's Constants[d]			R-Squared[c]	LOD
		Calibration Range[a] (mM)	Linear Regression Equation's Constants[b]		R-Squared[c]					
			A	B		A	B	α		
Tris buffer[f] (150 mM, pH 7.4)	Na^+	0-5	0.26	1.06	0.985	2.64	1.5	0.13	0.99	0.77
	K^+	0-1	0.51	1.03	0.958	3.79	2.12	0.017	0.88	0.33
	Ca^{2+}	0-4	0.086	1.01	0.955	1.45	0.46	0.31	0.97	0.99
Artificial urine[e] (pH 6)	Na^+	0-10	0.13	1.01	0.978	7.13	6.11	0.024	0.997	1.90
	K^+	0-10	0.03	1.02	0.962	2.36	1.36	0.031	0.989	2.39
	Ca^{2+}	0-2	0.11	1.01	0.854	1.43	0.39	0.256	0.922	1.13
Artificial urine[f] (pH 6)	Na^+	0-5	0.106	0.65	0.97	1.54	0.91	0.15	0.99	1.26
	K^+	10-150	0.0198	1.16	0.99	-				0.85
	Ca^{2+}	0.5-10	0.0166	0.19	0.99	-				1.2

** Number of measurements = 6
a Actual linear range is wider
b Linear Regression Equation is: $\frac{I}{I_0} = A \times C + B$, where A and B are constant and C is the concentration (mM)
c Correlation coefficient
d Exponential Equation is: $\frac{I}{I_0} = A - Be^{-\alpha C}$
e Plate reader is used for measuring the concentration of ions
f Smartphone-based device is used for measuring the concentration of ions

Limit of detection (LOD) for measuring the concentration of ions was calculated according to the following formula[111]:

$$LOD = 3\left(\frac{S_y}{S}\right) \quad (2)$$

where S_y is the standard deviation of the response of the linear curve and S is the slope of the linear calibration curve.

The LOD and calibration parameters of Na^+, K^+ and Ca^{2+} ions in Tris buffer (150 mM, pH 7.4) are summarized in Table 4-1.

To quantify the concentration of chloride and nitrite ions, the RGB model, as one of the most common methods for color detection, was used. In RGB images, there are three color channels; Red, Green, and Blue. In most cases, the colors present in the images

are a combination of all three channels. Figure 4-4d,e, which present the component of the RGB model for different concentrations of chloride and nitrite ions, respectively, show that the intensity changes mostly occur in the red and blue channels, respectively; therefore, these channels have the highest sensitivity. LOD of the nitrite ion using the blue channel was 0.239 mM.

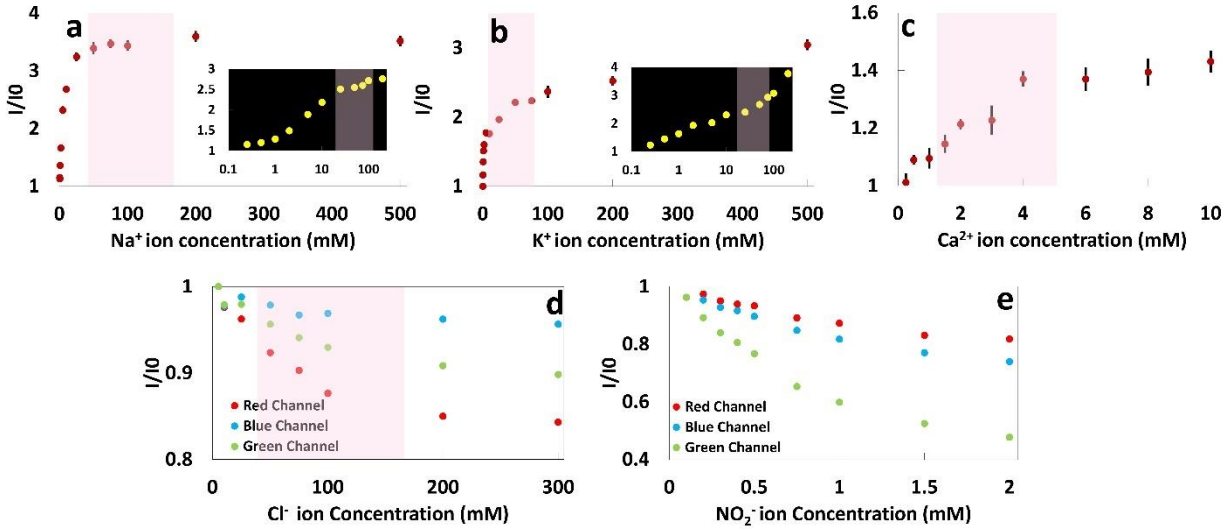

Figure 4-4. Na^+, K^+, Ca^{2+}, Cl^-, and NO_2^- ion concentration measurements in Tris buffer (150 mM, pH 7.4) using fluorescent probes (Sodium Green, PBFI, and Fluzin, respectively) and the RGB model*. Calibration curves of (a) Na^+,(b) K^+, and (c) Ca^{2+} ions on paper matrix at a constant probe concentration of 25 μM in DMSO (Sodium Green ($\lambda_{ex}/\lambda_{em}$: 485/541 nm), PBFI ($\lambda_{ex}/\lambda_{em}$: 360/450 nm), and Fluzin ($\lambda_{ex}/\lambda_{em}$: 485/541 nm)). Red, Blue, and Green channels of the RGB model for different concentrations of (d) Cl^- and (e) NO_2^- ions. Insets in (a) and (b) show the logarithmic scale of Na^+ and K^+ concentrations, respectively. Error bars represent standard error of the mean (n=6). Pink shaded area shows the physiological ion concentration ranges in human urine.*

Detecting electrolytes in artificial urine

To simulate human urine, an artificial urine solution with a wide range of ion concentrations was synthesized. Figure 4-5 shows the results of detecting Na^+, K^+, Ca^{2+}, Cl^-, and NO_2^- ions in artificial urine. The fluorescent intensity of the cations was measured using a plate reader. It can be seen that by increasing the concentration of cations,

fluorescent intensities increase. Using Eq. 1, the saturation decay ($\propto$) of Na^+, K^+, and Ca^{2+} ions in artificial urine was calculated. The saturation decay and R-squared values are summarized in Table 4-1. These results clearly demonstrated that Na^+, K^+, and Ca^{2+} ions in urine can be detected with high precision. Increasing the concentration of Na^+ and K^+ from 50 to 250 mM and from 5 to 150 mM within the physiological range led to a 31.4% and 82.3% increase in their fluorescent probe intensity, respectively. Moreover, by increasing the concentration of Ca^{2+} within the physiological range (1 to 10 mM), the fluorescent intensity of Fluozin increased 17.11%. The calibration parameters and limit of detection of Na^+, K^+, and Ca^{2+} are summarized in Table 4-1. Furthermore, Figure 4-5d shows the results of detecting Cl^- in artificial urine using 4 µl of reagent following by adding 2 µl of sample containing the Cl^- ion at different concentrations. It can be seen that red channel had the highest sensitivity. Moreover, the results of Figure 4-5e show that the nitrite ion with a concentration as low as 50 µM can be detected in artificial urine and the calculated LOD based on the results of the blue channel was 0.13 mM.

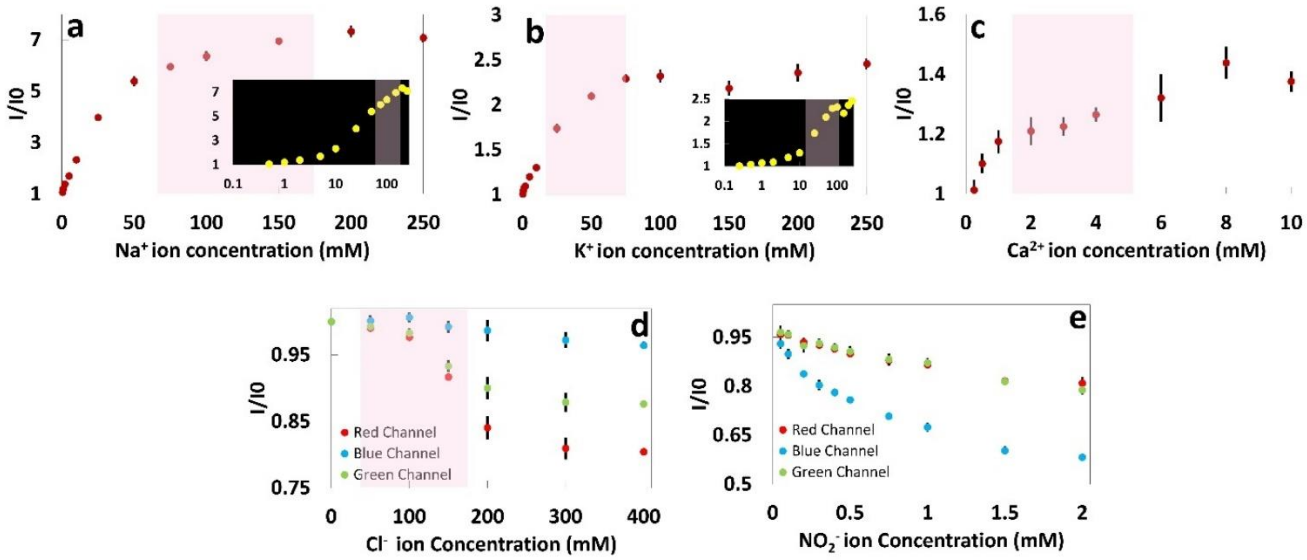

Figure 4-5. Na+, K+, Ca2+, Cl-, and NO_2^- ion measurements in artificial urine (pH 6) using fluorescent probes (Sodium Green, PBFI, and Fluzin, respectively) and the RGB model. *Calibration curves of (a) Na^+,(b) K^+, and Ca^{2+} ions on paper matrix at a constant probe concentration of 25 µM in DMSO (Sodium Green ($\lambda_{ex}/\lambda_{em}$: 485/541 nm), PBFI ($\lambda_{ex}/\lambda_{em}$: 360/450 nm), and Fluzin ($\lambda_{ex}/\lambda_{em}$: 485/541 nm)). Red, Blue, and Green channels of the RGB model for different concentrations of (d) Cl^- and (e) NO_2^- ions. Insets in (a) and (b) show the logarithmic scale of Na^+ and K^+ concentrations, respectively. Error bars represent standard error of the mean (n=6). Pink shaded area shows the physiological ion concentration ranges in human urine.*

Finally, the plate reader was replaced with the developed smartphone-based platform and measured the concentration of ions. Figure 4-6 shows the fluorescent intensity of the probes in the presence of different ion concentrations. Calibration parameters and LOD of Na^+, K^+, and Ca^{2+} in artificial urine are summarized in Table 4-1.

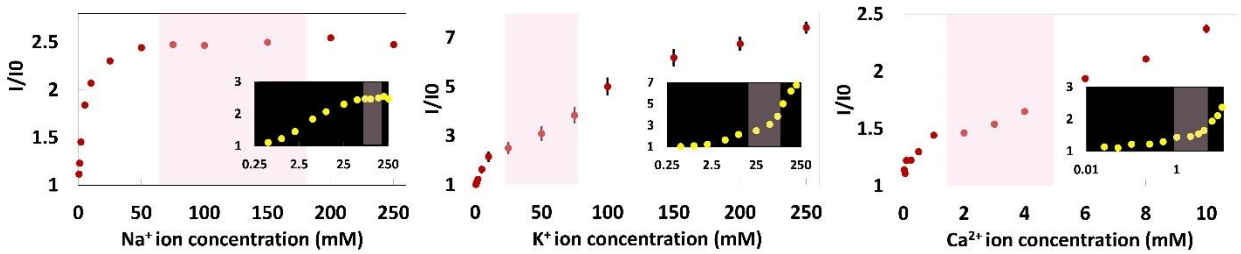

Figure 4-6. Na^+, K^+, and Ca^{2+} ion measurements in artificial urine (pH 6) using fluorescent probes (Sodium Green, PBFI, and Fluzin, respectively). *Calibration curves of (a) Na^+,(b) K^+, and Ca^{2+} ions on paper matrix at a constant probe concentration of 250 µM in DMSO (Sodium Green ($\lambda_{ex}/\lambda_{em}$: 485/541 nm), PBFI ($\lambda_{ex}/\lambda_{em}$: 360/450 nm), and Fluzin ($\lambda_{ex}/\lambda_{em}$: 485/541 nm)). Insets show the logarithmic scale of Na^+, K^+, and Ca^{2+} concentrations, respectively. Error bars represent standard error of the mean (n=6). Pink shaded area shows the physiological ion concentration ranges in human urine.*

<u>*Conclusions*</u>

To address the importance of measuring the concentration of electrolytes, such as Na^+, K^+, Ca^{2+}, Cl^-, and NO_2^- ions in body fluid, especially for the people with blood pressure issues and kidney diseases who need to regularly track their intake of sodium, potassium and calcium, a smartphone-based device was proposed for quantifying the concentration of these ions in urine. Using this method, the ability of using a miniaturized paper-based, smartphone-enabled device for quantification of electrolytes in artificial urine by fluorescent and colorimetric detection methods was demonstrated. By using this cost-effective device, daily quantification of ions in urine would be feasible, which can result in both monetary and time savings for people needing regular detection. The proposed device can be further utilized for diagnosing diseases such as hypertension, hyperkalemia or hypokalemia, kidney disease, cystic fibrosis, and urinary tract infection (UTI) by measuring the concentration of Na^+, K^+, Ca^{2+}, Cl^-, and NO_2^- ion in urine.

Conclusion

This thesis introduced a low-cost and high-throughput fabrication method for paper-based microfluidic diagnostic devices, using a pen plotter and hydrophobic marker. Several commercially-available hydrophobic markers were tested and two types of paper to choose the best ones for fabricating the paper-based microfluidic devices. At the first step, the pen-plotter was integrated with a paper-feeder to have a mass-production process. Then, a 3D-printed multi-pen holder was integrated for drawing several patterns at the same time instead of one. Moreover, the hydrophobic marker was substituted with a technical pen connected to an ink reservoir. In fact, a continuous ink system was used in line with the purpose for having a high-throughput fabrication method. To demonstrate the potential bio-chemical analytical capabilities of the fabrication method, six colorimetric biological assays were conducted: glucose, nitrite, urobilinogen, protein, blood, and pH. The fabrication method proposed here offers low cost, rapid, and simple fabrication of high-resolution paper-based microfluidic devices, which can be useful for mass production in both resource-limited and developed countries.

Then, the proposed method was used for fabricating electrochemical paper-based microfluidic devices. Conductive ink was used for patterning the electrodes of the device and hydrophobic marker was used for defining the hydrophobic barrier. Glucose assay was also conducted to show the potential capability of the suggested fabrication method. At the next step, a cell-phone based platform was designed using miniaturized paper-based devices for measuring the concentration of ions in artificial urine. In this step, fluorescent detection method was used and it was shown that the concentration of ions (sodium, potassium, calcium, chloride, and nitrite) in the physiological range can be successfully measured.

Overall, a low-cost, high-throughput method was developed for fabrication of paper-based microfluidic devices for diagnostic purposes. Its validation was shown by conducting urine analysis assays via different detection methods such as colorimetric, electrochemical and fluorescent methods.

Reference

1. See National Science Foundation, for Smart and Connected Health (SCH). (2016). Available at: https://www.nsf.gov/funding/pgm_summ.jsp?pims_id=504739.
2. See The World Bank, for Health expenditure per capita (current US$). (2015). Available at: https://www.oecd.org/health/health-systems/Focus-Health-Spending-2015.pdf .
3. Maciosek, M. V., Coffield, A. B., Flottemesch, T. J., Edwards, N. M. & Solberg, L. I. Greater use of preventive services in U.S. health care could save lives at little or no cost. *Health Aff.* (2010). doi:10.1377/hlthaff.2008.0701
4. Bladder and Bowel Community, for Bladder Conditions and Symptoms.
5. Simerville, J. A., Maxted, W. C. & Pahira, J. J. Urinalysis: a comprehensive review. *Am. Fam. Physician 71*(6), 1153-62 (2005).
6. Lepowsky, E., Ghaderinezhad, F., Knowlton, S. & Tasoglu, S. Paper-based assays for urine analysis. *Biomicrofluidics* 11, 051501 (2017).
7. Yetisen, A. K., Akram, M. S. & Lowe, C. R. Paper-based microfluidic point-of-care diagnostic devices. *Lab Chip* 13, 2210–2251 (2013).
8. Martinez, A. W., Phillips, S. T., Whitesides, G. M., Carrilho, E. & Chem, A. Diagnostics for the developing world: microfluidic paper-based analytical devices. *Anal. Chem.* 82, 3–10 (2010).
9. Ghaderinezhad, F. *et al.* High-throughput rapid-prototyping of low-cost paper-based microfluidics. *Sci. Rep.* 7, 3553 (2017).
10. Martinez, A. W., Phillips, S. T., Butte, M. J. & Whitesides, G. M. Patterned paper as a platform for inexpensive, low-volume, portable bioassays. *Angew. Chemie - Int. Ed. 46*(8), 1318-1320 (2007). doi:10.1002/anie.200603817
11. Abe, K., Suzuki, K. & Citterio, D. Inkjet-Printed Microfluidic Multianalyte Chemical Sensing Paper. 80, 6928–6934 (2008).
12. Lu, Y., Shi, W., Qin, J. & Lin, B. Fabrication and Characterization of Paper-Based Microfluidics Prepared in Nitrocellulose Membrane By Wax Printing. *Anal. Chem.* 82, 329–335 (2010).
13. Lu, R., Shi, W., Jiang, L., Qin, J. & Lin, B. Rapid prototyping of paper-based microfluidics with wax for low-cost, portable bioassay. *Electrophoresis 30*(9), 1497-1500 (2009). doi:10.1002/elps.200800563
14. Xu, C., Cai, L., Zhong, M. & Zheng, S. Low-cost and rapid prototyping of microfluidic paper-based analytical devices by inkjet printing of permanent marker ink. *RSC Adv. 5*(7), 4770-4773 (2015). doi:10.1039/c4ra13195a
15. Bruzewicz, D. A., Reches, M. & Whitesides, G. M. Low-cost printing of poly(dimethylsiloxane) barriers to define microchannels in paper. *Anal. Chem. 80*(9), 3387-3392 (2008). doi:10.1021/ac702605a
16. Li, X., Tian, J., Garnier, G. & Shen, W. Fabrication of paper-based microfluidic sensors by printing. *Colloids Surfaces B Biointerfaces 76*(2), 564-570 (2010). doi:10.1016/j.colsurfb.2009.12.023
17. Li, X., Tian, J., Nguyen, T. & Shen, W. Paper-based microfluidic devices by plasma treatment. *Anal. Chem. 80*(23), 9131-9134 (2008). doi:10.1021/ac801729t
18. World Health Organization (WHO). Increasing Access to Diagnostics Through Technology Transfer and Local Production. 1–44 (2011).

19. Wong, V. L. *et al.* A Paper-Based Multiplexed Transaminase Test for Low-Cost, Point-of-Care Liver Function Testing. *Sci. Transl. Med.* 4, 152ra129-152ra129 (2012).
20. Amin, R. *et al.* Continuous-Ink, Multiplexed Pen-Plotter Approach for Low-Cost, High-Throughput Fabrication of Paper-Based Microfluidics. *Anal. Chem.* 89, 6351–6357 (2017).
21. Songjaroen, T., Dungchai, W., Chailapakul, O., Henry, C. S. & Laiwattanapaisal, W. Blood separation on microfluidic paper-based analytical devices. *Lab Chip 12*(18), 3392-3398 (2012). doi:10.1039/c2lc21299d
22. Tian, L. *et al.* Bioplasmonic paper as a platform for detection of kidney cancer biomarkers. *Anal. Chem.* 84, 9928–9934 (2012).
23. Mentele, M. M., Cunningham, J., Koehler, K., Volckens, J. & Henry, C. S. Microfluidic paper-based analytical device for particulate metals. *Anal. Chem.* 84, 4474–4480 (2012).
24. Sameenoi, Y. *et al.* Microfluidic paper-based analytical device for aerosol oxidative activity. *Environ. Sci. Technol. 47*(2), 932-940 (2013). doi:10.1021/es304662w
25. Jokerst, J. C. *et al.* Development of a paper-based analytical device for colorimetric detection of select foodborne pathogens. *Anal. Chem.* 84, 2900–2907 (2012).
26. He, Q., Ma, C., Hu, X. & Chen, H. Method for fabrication of paper-based microfluidic devices by alkylsilane self-assembling and UV/O3-patterning. *Anal. Chem.* 85, 1327–1331 (2013).
27. Hossain, S. M. Z., Luckham, R. E., McFadden, M. J. & Brennan, J. D. Reagentless bidirectional lateral flow bioactive paper sensors for detection of pesticides in beverage and food samples. *Anal. Chem. 81*(21), 9055-9064 (2009). doi:10.1021/ac901714h
28. Cai, L., Wu, Y., Xu, C. & Chen, Z. A simple paper-based microfluidic device for the determination of the total amino acid content in a tea leaf extract. *J. Chem. Educ. 90*(2), 232-234 (2013). doi:10.1021/ed300385j
29. Sechi, D., Greer, B., Johnson, J. & Hashemi, N. Three-Dimensional Paper-Based Microfluidic Device for Assays of Protein and Glucose in Urine. *Anal. Chem.* 85, 10733–10737 (2013).
30. De Tarso Garcia, P., Garcia Cardoso, T. M., Garcia, C. D., Carrilho, E. & Tomazelli Coltro, W. K. A handheld stamping process to fabricate microfluidic paper-based analytical devices with chemically modified surface for clinical assays. *RSC Adv. 4*(71), 37637-37644 (2014). doi:10.1039/c4ra07112c
31. Olkkonen, J., Lehtinen, K. & Erho, T. Flexographically printed fluidic structures in paper. *Anal. Chem.* 82, 10246–10250 (2010).
32. Sones, C. L. *et al.* Laser-induced photo-polymerisation for creation of paper-based fluidic devices. *Lab Chip 14*(23), 4567-4574 (2014). doi:10.1039/c4lc00850b
33. Chitnis, G., Ding, Z., Chang, C. L., Savran, C. A. & Ziaie, B. Laser-treated hydrophobic paper: An inexpensive microfluidic platform. in *Lab on a Chip 11*(6), 1161-1165 (2011). doi:10.1039/c0lc00512f
34. Xia, Y., Si, J. & Li, Z. Fabrication techniques for microfluidic paper-based

analytical devices and their applications for biological testing: A review. *Biosens. Bioelectron.* 77, 774–789 (2016).
35. He, Y., Wu, Y., Fu, J. Z. & Wu, W. Bin. Fabrication of paper-based microfluidic analysis devices: a review. *RSC Adv.* 5, 78109–78127 (2015).
36. Peele, J. D., Gadsden, R. H. & Crews, R. Semi-automated vs. Visual reading of urinalysis dipsticks. *Clin. Chem. 23*(12), 2242-2246 (1977).
37. Raba, J. & Mottola, H. A. Glucose Oxidase as an Analytical Reagent. *Crit. Rev. Anal. Chem. 25*(1), 1-42 (1995). doi:10.1080/10408349508050556
38. Martinez, A. W. *et al.* Simple telemedicine for developing regions: Camera phones and paper-based microfluidic devices for real-time, off-site diagnosis. *Anal. Chem. 80*(10), 3699-3707 (2008). doi:10.1021/ac800112r
39. Nie, J. *et al.* Low-cost fabrication of paper-based microfluidic devices by one-step plotting. *Anal. Chem. 84*(15), 6331-6335 (2012). doi:10.1021/ac203496c
40. Anciaux, S. K., Geiger, M. & Bowser, M. T. 3D Printed Micro Free-Flow Electrophoresis Device. *Anal. Chem. 88*(15), 7675-7682 (2016). doi:10.1021/acs.analchem.6b01573
41. Bruno, G. *et al.* The active modulation of drug release by an ionic field effect transistor for an ultra-low power implantable nanofluidic system. *Nanoscale 8*(44), 18718-18725 (2016). doi:10.1039/c6nr06235k
42. Liang, Y. R. *et al.* 3D-Printed High-Density Droplet Array Chip for Miniaturized Protein Crystallization Screening under Vapor Diffusion Mode. *ACS Appl. Mater. Interfaces 9*(13), 11837-11845 (2017). doi:10.1021/acsami.6b15933
43. Macdonald, N. P. *et al.* Comparing Microfluidic Performance of Three-Dimensional (3D) Printing Platforms. *Anal. Chem. 89*(7), 3858-3866 (2017). doi:10.1021/acs.analchem.7b00136
44. Amin, R., Knowlton, S., Hart, A., Yenilmez, B. & Ghaderinezhad, F. 3D-printed microfluidic devices. 8, 022001 (2016).
45. Sivashankar, S. *et al.* Compatibility analysis of 3D printer resin for biological applications. *Micro Nano Lett. 11*(10), 654-659 (2016). doi:10.1049/mnl.2016.0530
46. Amin, R., Li, L. & Tasoglu, S. Assessing reusability of microfluidic devices: Urinary protein uptake by PDMS-based channels after long-term cyclic use. *Talanta* 192, 455-462 (2019). doi:10.1016/j.talanta.2018.08.053
47. Lepowsky, E., Amin, R. & Tasoglu, S. Assessing the Reusability of 3D-Printed Photopolymer Microfluidic Chips for Urine Processing. *Micromachines* 9 (10), 520 (2018). doi:10.3390/mi9100520
48. Amin, R. *et al.* 3D-printed smartphone-based device for label-free cell separation. *J. 3D Print. Med.* 1 (3), 155-164 (2017). doi:10.2217/3dp-2016-0007
49. Knowlton, S., Joshi, A., Syrrist, P., Coskun, A. F. & Tasoglu, S. 3D-printed smartphone-based point of care tool for fluorescence- and magnetophoresis-based cytometry. *Lab Chip* 17 (16), 2839-2851 (2017). doi:10.1039/c7lc00706j
50. Yenilmez, B., Knowlton, S. & Tasoglu, S. Self-Contained Handheld Magnetic Platform for Point of Care Cytometry in Biological Samples. *Adv. Mater. Technol.* 1 (9), 1600144 (2016). doi:10.1002/admt.201600144
51. Yenilmez, B., Knowlton, S., Yu, C. H., Heeney, M. M. & Tasoglu, S. Label-Free Sickle Cell Disease Diagnosis using a Low-Cost, Handheld Platform. *Adv. Mater.*

Technol. 1 (5), 1600100 (2016). doi:10.1002/admt.201600100
52. Knowlton, S. *et al.* 3D-printed microfluidic chips with patterned, cell-laden hydrogel constructs. *Biofabrication* 8 (2), 025019 (2016). doi:10.1088/1758-5090/8/2/025019
53. Amin, R. *et al.* Smart-phone attachable, flow-assisted magnetic focusing device. *RSC Adv.* 6 (96), 93922-93931 (2016). doi:10.1039/c6ra19483d
54. Knowlton, S. *et al.* Advancing cancer research using bioprinting for tumor-on-a-chip platforms. *Int. J. Bioprinting* 2 (2), 3-8 (2017). doi:10.18063/ijb.2016.02.003
55. Knowlton, S., Yenilmez, B. & Tasoglu, S. Towards Single-Step Biofabrication of Organs on a Chip via 3D Printing. *Trends in Biotechnology* 34 (9), 685-688 (2016). doi:10.1016/j.tibtech.2016.06.005
56. Knowlton, S., Yu, C. H., Jain, N., Ghiran, I. C. & Tasoglu, S. Smart-phone based magnetic levitation for measuring densities. *PLoS One* 10 (8), e0134400 (2015). doi:10.1371/journal.pone.0134400
57. Knowlton, S. & Tasoglu, S. A Bioprinted Liver-on-a-Chip for Drug Screening Applications. *Trends in Biotechnology* 34 (9), 681-682 (2016). doi:10.1016/j.tibtech.2016.05.014
58. Luo, Z. Y. *et al.* Deformation of a single mouse oocyte in a constricted microfluidic channel. *Microfluid. Nanofluidics* 19 (4), 883-890 (2015). doi:10.1007/s10404-015-1614-0
59. Knowlton, S. M., Sadasivam, M. & Tasoglu, S. Microfluidics for sperm research. *Trends in Biotechnology* 33 (4), 221-229 (2015). doi:10.1016/j.tibtech.2015.01.005
60. Whitesides, G. M. The origins and the future of microfluidics. *Nature 442*(7101), 368 (2006). doi:10.1038/nature05058
61. Li, X., Tian, J. & Shen, W. Quantitative biomarker assay with microfluidic paper-based analytical devices. *Anal. Bioanal. Chem. 396*(1), 495-501 (2010). doi:10.1007/s00216-009-3195-9
62. Carrilho, E., Martinez, A. W. & Whitesides, G. M. Understanding wax printing: a simple micropatterning process for paper-based microfluidics. *Anal. Chem.* 81, 7091–7095 (2009).
63. Klasner, S. A. *et al.* Paper-based microfluidic devices for analysis of clinically relevant analytes present in urine and saliva. *Anal. Bioanal. Chem. 397*(5), 1821-1829 (2010). doi:10.1007/s00216-010-3718-4
64. Lin, S. C. *et al.* Cotton-based diagnostic devices. *Sci. Rep. 4*, 6976 (2014). doi:10.1038/srep06976
65. Xia, Y., Si, J. & Li, Z. Fabrication techniques for microfluidic paper-based analytical devices and their applications for biological testing: A review. *Biosensors and Bioelectronics 77*, 774-789 (2016). doi:10.1016/j.bios.2015.10.032
66. Metters, J. P., Houssein, S. M., Kampouris, D. K. & Banks, C. E. Paper-based electroanalytical sensing platforms. *Anal. Methods 5*(1), 103-110 (2013). doi:10.1039/c2ay26396c
67. Zhao, C., Thuo, M. M. & Liu, X. A microfluidic paper-based electrochemical biosensor array for multiplexed detection of metabolic biomarkers. *Sci. Technol. Adv. Mater. 14*(5), 054402 (2013). doi:10.1088/1468-6996/14/5/054402

68. Li, B. *et al.* Controlling Capillary-Driven Fluid Transport in Paper-Based Microfluidic Devices Using a Movable Valve. *Anal. Chem. 89*(11), 5707-5712 (2017). doi:10.1021/acs.analchem.7b00726
69. Morbioli, G. G., Mazzu-Nascimento, T., Milan, L. A., Stockton, A. M. & Carrilho, E. Improving Sample Distribution Homogeneity in Three-Dimensional Microfluidic Paper-Based Analytical Devices by Rational Device Design. *Anal. Chem.* 89, 4786–4792 (2017).
70. Rahbar, M., Nesterenko, P. N., Paull, B. & Macka, M. Geometrical Alignment of Multiple Fabrication Steps for Rapid Prototyping of Microfluidic Paper-Based Analytical Devices. *Anal. Chem.* 3-10 (2017). doi:10.1021/acs.analchem.7b03796
71. Li, Z. *et al.* Direct writing electrodes using a ball pen for paper-based point-of-care testing. *Analyst 140*(16), 5526-5535 (2015). doi:10.1039/c5an00620a
72. Dungchai, W., Chailapakul, O. & Henry, C. S. Electrochemical detection for paper-based microfluidics. *Anal. Chem. 81*(14), 5821-5826 (2009). doi:10.1021/ac9007573
73. Yang, Y. *et al.* Paper-Based Microfluidic Devices: Emerging Themes and Applications. *Anal. Chem.* 89, 71–91 (2017).
74. Shiroma, L. Y., Santhiago, M., Gobbi, A. L. & Kubota, L. T. Separation and electrochemical detection of paracetamol and 4-aminophenol in a paper-based microfluidic device. *Anal. Chim. Acta 725*, 44-50 (2012). doi:10.1016/j.aca.2012.03.011
75. Liana, D. D. *et al.* Sintered gold nanoparticles as an electrode material for paper-based electrochemical sensors. *RSC Adv. 3*(23), 8683-8691 (2013). doi:10.1039/c3ra00102d
76. Hu, C. *et al.* Inkjet printing of nanoporous gold electrode arrays on cellulose membranes for high-sensitive paper-like electrochemical oxygen sensors using ionic liquid electrolytes. *Anal. Chem. 84*(8), 3745-3750 (2012). doi:10.1021/ac3003243
77. Ruecha, N., Chailapakul, O., Suzuki, K. & Citterio, D. Fully Inkjet-Printed Paper-Based Potentiometric Ion-Sensing Devices. *Anal. Chem.* 89, 10608–10616 (2017).
78. Nie, Z., Deiss, F., Liu, X., Akbulut, O. & Whitesides, G. M. Integration of paper-based microfluidic devices with commercial electrochemical readers. *Lab Chip 10*(22), 3163-3169 (2010). doi:10.1039/c0lc00237b
79. Dossi, N. *et al.* Pencil-drawn paper supported electrodes as simple electrochemical detectors for paper-based fluidic devices. *Electrophoresis 34*(14), 2085-2091 (2013). doi:10.1002/elps.201200425
80. Russo, A. *et al.* Pen-on-paper flexible electronics. *Adv. Mater. 23*(30), 3426-3430 (2011). doi:10.1002/adma.201101328
81. Ghosale, A., Shrivas, K., Shankar, R. & Ganesan, V. Low-Cost Paper Electrode Fabricated by Direct Writing with Silver Nanoparticle-Based Ink for Detection of Hydrogen Peroxide in Wastewater. *Anal. Chem. 89*(1), 776-782 (2017). doi:10.1021/acs.analchem.6b03512
82. Wang, J. *Analytical Electrochemistry, Third Edition*. *Analytical Electrochemistry, Third Edition* (2006). doi:10.1002/0471790303
83. Nie, Z. *et al.* Electrochemical sensing in paper-based microfluidic devices. *Lab*

Chip (2010). doi:10.1039/b917150a
84. Brownson, D. A. C., Banks, C. E., Brownson, D. A. C. & Banks, C. E. Interpreting Electrochemistry. in *The Handbook of Graphene Electrochemistry* (2014). doi:10.1007/978-1-4471-6428-9_2
85. Wan, Q. J., Kubáň, P., Tanyanyiwa, J., Rainelli, A. & Hauser, P. C. Determination of major inorganic ions in blood serum and urine by capillary electrophoresis with contactless conductivity detection. *Anal. Chim. Acta* 525, 11–16 (2004).
86. Gonçalves, C. *et al.* Sodium and potassium urinary excretion and dietary intake: A cross-sectional analysis in adolescents. *Food Nutr. Res.* 60, 1–11 (2016).
87. Viera, A. J. & Wouk, N. Potassium disorders: Hypokalemia and hyperkalemia. *Am. Fam. Physician* 92, 487–495 (2015).
88. Mizéhoun-Adissoda, C. *et al.* Estimation of Daily Sodium and Potassium Excretion Using Spot Urine and 24-Hour Urine Samples in a Black Population (Benin). *J. Clin. Hypertens.* 18, 634–640 (2016).
89. Anthony J. Viera, and N. W. *Potassium Disorders: Hypokalemia and Hyperkalemia*. *American Family Physician* 91, (American Academy of Family Physicians, 1970).
90. Foley, K. F. & Boccuzzi, L. Urine Calcium: Laboratory Measurement and Clinical Utility. *Lab. Med.* 41, 683–686 (2010).
91. Cirillo, M., Laurenzi, M., Panarelli, W. & Stamler, J. Urinary sodium to potassium ratio and urinary stone disease. The Gubbio Population Study Research Group. *Kidney Int.* 46, 1133–1139 (1994).
92. Pirkle, J. L. Laboratory Procedure Manual, Sodium , Potassium , Chloride Urine. *Natl. Cent. Environ. Heal.* (2016).
93. Schmiemann, G., Kniehl, E., Gebhardt, K., Matejczyk, M. M. & Hummers-Pradier, E. The diagnosis of urinary tract infection. *Pediatrics* 107, 361–367 (2010).
94. Butler, A. R. & Feelisch, M. Therapeutic uses of inorganic nitrite and nitrate: From the past to the future. *Circulation* 117, 2151–2159 (2008).
95. Subramanian, A., Rangarajan, K., Pandey, R. & Albert, V. Agreement of two different laboratory methods used to measure electrolytes. *J. Lab. Physicians* 3, 104 (2011).
96. West, P. An evaluation of the AM 721 ion-selective electrode system for the estimation of sodium and potassium in plasma , urine and whole blood. 5, 182–187 (1983).
97. Chapp, A. D. *et al.* Measurement of cations, anions, and acetate in serum, urine, cerebrospinal fluid, and tissue by ion chromatography. *Physiol. Rep.* 6, 1–15 (2018).
98. Rhemrev-Boom, M. M. Determination of anions with capillary electrophoresis and indirect ultraviolet detection. *J. Chromatogr. A* 680, 675–684 (1994).
99. Olsšauskaite, V., Paliulionyte, V. & Padarauskas, A. Rapid analysis of cation constituents of urine by capillary electrophoresis. *Clin. Chim. Acta* 293, 181–186 (2000).
100. Li, H., Han, D., Pauletti, G. M. & Steckl, A. J. Blood coagulation screening using a paper-based microfluidic lateral flow device. *Lab Chip* 14, 4035–4041 (2014).
101. Zhang, Y., Zuo, P. & Ye, B. C. A low-cost and simple paper-based microfluidic device for simultaneous multiplex determination of different types of chemical

contaminants in food. *Biosens. Bioelectron.* 68, 14–19 (2015).
102. Ma, L., Nilghaz, A., Choi, J. R., Liu, X. & Lu, X. Rapid detection of clenbuterol in milk using microfluidic paper-based ELISA. *Food Chem.* 246, 437–441 (2018).
103. Meredith, N. A. *et al.* Paper-based analytical devices for environmental analysis. *Analyst* 141, 1874–1887 (2016).
104. Gong, M. M. & Sinton, D. Turning the Page: Advancing Paper-Based Microfluidics for Broad Diagnostic Application. *Chem. Rev.* 117, 8447–8480 (2017).
105. Yamada, K., Shibata, H., Suzuki, K. & Citterio, D. Toward practical application of paper-based microfluidics for medical diagnostics: state-of-the-art and challenges. *Lab Chip* 17, 1206–1249 (2017).
106. Amin, R. *et al.* Continuous-Ink, Multiplexed Pen-Plotter Approach for Low-Cost, High-Throughput Fabrication of Paper-Based Microfluidics. *Anal. Chem* 89, 6351–6357 (2017).
107. Martinez, A. W., Phillips, S. T. & Whitesides, G. M. Three-dimensional microfluidic devices fabricated in layered paper and tape. *Proc. Natl. Acad. Sci.* 105, 19606–19611 (2008).
108. Wians, F. H. Urine Tests: Normal Values. (2016).
109. Yetisen, A. K. *et al.* Paper-based microfluidic system for tear electrolyte analysis. *Lab Chip* 17, 1137–1148 (2017).
110. Skoog, D. A., Holler, F. J., Crouch, S. R. *Principles of Instrumental Analysis*. (David Harris, 1992). doi:10.1109/ACSSC.2017.8335505
111. Ich. ICH Topic Q2 (R1) Validation of Analytical Procedures : Text and Methodology. *Int. Conf. Harmon.* 1994, 17 (2005).